bioRxiv preprint doi: https://doi.org/10.1101/2021.03.22.435957; this version posted March 22, 2021. The copyright holder for this preprint (which was not certified by peer review) is the author/funder, who has granted bioRxiv a license to display the preprint in perpetuity. It is made available under aCC-BY 4.0 International license.

Protease-activatable biosensors of SARS-CoV-2 infection for cell-based drug, neutralisation and virological assays

Pehuén Pereyra Gerber[1,2], Lidia M Duncan[1,2], Edward JD Greenwood[1,2], Sara Marelli[1,2], Adi Naamati[1,2], Ana Teixeira-Silva[1,2], Thomas WM Crozier[1,2], Ildar Gabaev[1,2], Jun R Zhan[1,2], Anna V Protasio[3], Nicholas J Matheson[1,2,4,*]

1. Department of Medicine, University of Cambridge, UK
2. Cambridge Institute for Therapeutic Immunology and Infectious Disease (CITIID), Jeffrey Cheah Biomedical Centre, University of Cambridge, UK
3. Department of Pathology, University of Cambridge, UK
4. NHS Blood and Transplant, Cambridge, UK

*Correspondence: njm25@cam.ac.uk

bioRxiv preprint doi: https://doi.org/10.1101/2021.03.22.435957; this version posted March 22, 2021. The copyright holder for this preprint (which was not certified by peer review) is the author/funder, who has granted bioRxiv a license to display the preprint in perpetuity. It is made available under aCC-BY 4.0 International license.

Abstract

The world is in the grip of a severe acute respiratory syndrome coronavirus 2 (SARS-CoV-2) pandemic, and there is an urgent unmet clinical need for effective antiviral therapies. Many inhibitors of viral enzymes identified *in vitro* have limited efficacy against viral replication in cells, but conventional plaque assays are impractical for high-throughput screens. In this study, we therefore engineer cell-based biosensors of SARS-CoV-2 infection. Our assays exploit the cleavage of specific oligopeptide linkers by SARS-CoV-2 Main or Papain-like proteases, leading to the activation of green fluorescent protein (GFP) or firefly luciferase-based reporters. First, we characterise these biosensors in cells using recombinant viral proteases. Next, we confirm their ability to detect endogenous viral protease expression during infection with wildtype SARS-CoV-2. Finally, we develop a sensitive luminescent reporter cell line, confirm that it accurately quantitates infectious SARS-CoV-2 virus, and demonstrate its utility for drug screening and titration of neutralising antibodies.

bioRxiv preprint doi: https://doi.org/10.1101/2021.03.22.435957; this version posted March 22, 2021. The copyright holder for this preprint (which was not certified by peer review) is the author/funder, who has granted bioRxiv a license to display the preprint in perpetuity. It is made available under aCC-BY 4.0 International license.

Introduction

Since its emergence in December 2019, SARS-CoV-2 has caused more than 100 million cases of coronavirus disease 2019 (COVID-19) and over 2 million deaths worldwide (https://ourworldindata.org/ [Online Resource]). Together with SARS-CoV and Middle East respiratory syndrome coronavirus (MERS-CoV), it is the third betacoronavirus to cause a large-scale human outbreak in the last two decades (V'Kovski et al., 2020). Even with effective vaccines, it is very likely that SARS-CoV-2 will continue to circulate and cause disease for the foreseeable future in at least some parts of the world (Phillips, 2021). The most promising direct-acting antiviral agent currently in the clinic is the RNA-dependent RNA polymerase inhibitor remdesivir, but it must be administered by intravenous infusion, and clinical trials have generated mixed results (Harrington et al., 2021). Research is therefore urgently required to identify and trial novel antiviral therapies against SARS-CoV-2 (Matheson and Lehner, 2020), as well as MERS-CoV and (potentially) future zoonotic coronaviruses.

Whilst direct, biochemical assays are commonly used for targeted drug discovery, the activity of small molecules *in vitro* often fails to translate to a cellular or *in vivo* context, because of factors such as membrane permeability, off-target effects and cytotoxicity (An and Tolliday, 2010). Cell-based assays have the potential to provide more physiologically relevant information, and allow the study of complex tertiary phenotypes such as viral replication. In fact, cell-based optical reporter systems have been instrumental in the development of antiviral therapies to combat a previous global pandemic, caused by human immunodeficiency virus-1 (HIV-1). Commensurate with this, more than a thousand publications have cited the luminescent and colorimetric HIV-1 reporter cell line TZM-bl (Wei et al., 2002), and over 700 have cited the fluorescent J-Lat model of HIV-1 latency (Jordan et al., 2003). These approaches have facilitated a wealth of fundamental research on retrovirology, and luciferase-based neutralisation assays in TZM-bl cells are used worldwide for the assessment of vaccine-elicited neutralising antibodies, monoclonal antibodies and the neutralising antibody response in HIV-1 infection (Sarzotti-Kelsoe et al., 2014).

bioRxiv preprint doi: https://doi.org/10.1101/2021.03.22.435957; this version posted March 22, 2021. The copyright holder for this preprint (which was not certified by peer review) is the author/funder, who has granted bioRxiv a license to display the preprint in perpetuity. It is made available under aCC-BY 4.0 International license.

Unlike HIV-1, relatively few tools are available to facilitate work with SARS-CoV-2. Conventional plaque reduction neutralisation tests (PRNT) remain the gold standard for quantification of viral replication, but the low throughput and long turnaround time of these assays limit their utility for large-scale screening of drugs or sera. Whilst fluorescent (Xie et al., 2020a) and luminescent (Xie et al., 2020b) SARS-CoV-2 reporter viruses have recently been described, the reconstruction and reverse genetic modification of full-length SARS-CoV-2 is laborious, and these approaches are therefore currently restricted to re-engineered reference strains, not emerging variants of concern (Walensky et al., 2021; Williams and Burgers, 2021). Likewise, lentiviral or vesicular stomatitis virus particles pseudotyped with the spike protein of SARS-CoV-2 may be substituted in some settings (Hyseni et al., 2020; Nie et al., 2020), but these assays are typically not standardised between laboratories, are only applicable to studies of viral entry, and correlate imperfectly with assays using authentic virus (Donal et al., 2021; Mishra et al., 2021). There is therefore an urgent unmet need for a simple, high-throughput cell-based assay, to quantitate authentic SARS-CoV-2 infection, including new clinical variants.

During the SARS-CoV-2 replication cycle, the 30 kb single-stranded positive-sense genomic RNA is used as a template to generate the polyproteins 1a and 1ab (pp1a and pp1ab). In turn, these polyproteins are processed into the 16 non-structural proteins (nsp1 to nsp16) by the action of two virally-encoded proteases on sequence-specific cleavage sites: the Papain-like Protease (PLPro or nsp3) and the Main or 3C-like Protease (MPro or nsp5) (Chen et al., 2020). Inhibitors of SARS-CoV-2 proteases are therefore candidate antiviral therapeutics (Jin et al., 2020b; Kneller et al., 2020; Ma et al., 2020; Shin et al., 2020; Vuong et al., 2020). Additionally, viral protease activity may be exploited for cell-based assays, through the use of protease-activatable biosensors. These assays typically depend on the cleavage of specific oligopeptide linkers, leading to the activation of fluorescent or luminescent reporter proteins. They have hitherto been used for the detection of over-expressed, recombinant proteases from diverse viruses including HIV-1, HCV, DENV-1, and MERS-CoV (Arias-Arias et al., 2020;

bioRxiv preprint doi: https://doi.org/10.1101/2021.03.22.435957; this version posted March 22, 2021. The copyright holder for this preprint (which was not certified by peer review) is the author/funder, who has granted bioRxiv a license to display the preprint in perpetuity. It is made available under aCC-BY 4.0 International license.

Kilianski et al., 2013; Lindsten et al., 2001; Sabariegos et al., 2009), but not endogenous viral protease expression during authentic infection.

In this study, we aim to exploit the presence of viral protease activity for the detection of authentic SARS-CoV-2 infection. We therefore generate protease-activatable fluorescent and luminescent biosensors for SARS-CoV-2 MPro and PLPro activity, one based on “flip” GFP (FlipGFP) (Zhang et al., 2019), and the other based on circularly permuted firefly luciferase (FFluc) (Wigdal et al., 2008). Having confirmed the specificity and utility of these reporters using recombinant viral proteases, we establish their ability to detect and quantitate infected cells. Finally, we develop a stable, luminescent reporter cell line, in which FFluc is activated by PLPro expression during SARS-CoV-2 infection. We demonstrate the utility of these cells in assays of small molecule antivirals and neutralising antibodies using a wildtype SARS-CoV-2 isolate.

bioRxiv preprint doi: https://doi.org/10.1101/2021.03.22.435957; this version posted March 22, 2021. The copyright holder for this preprint (which was not certified by peer review) is the author/funder, who has granted bioRxiv a license to display the preprint in perpetuity. It is made available under aCC-BY 4.0 International license.

Results

Generation of FlipGFP-based SARS-CoV-2 protease reporters

The FlipGFP reporter comprises a split, superfolder eGFP molecule in which the last two beta-sheets (10 and 11) are held in an inactive, parallel orientation by the coiled-coil domains K5 and E5 and a protease-cleavable oligopeptide linker (Zhang et al., 2019). After cleavage of this linker, the beta-sheets adopt an anti-parallel orientation and self-assemble with beta-sheets 1-9, restoring GFP fluorescence (**Figure 1A**).

To generate SARS-CoV-2 protease reporters, we replaced a tobacco etch virus (TEV) protease cleavage site present in the original FlipGFP oligopeptide linker with candidate MPro or PLPro cleavage sites from the pp1a polyprotein of SARS-CoV-2 (**Figure 1B**). For MPro, we selected a wildtype self-cleavage sequence (SAVLQ/SGF, herein termed WT3c) present between nsp4 and nsp5, and an “optimal” cleavage sequence (TVRLQ/SGF, herein termed Opt3c) found by substrate profiling of SARS-CoV MPro (Chuck et al., 2010), and subsequently validated for SARS-CoV-2 MPro (Wioletta Rut, BiorXiv). For PLPro, we selected all three cognate cleavage sequences present in the pp1a polyprotein (ELNGG/AYT, herein termed PLP1; TLKGG/APT, herein termed PLP2; and ALKGG/KIV, herein termed PLP3). Importantly, all the wildtype sequences tested are highly conserved amongst SARS-CoV-2 and SARS-CoV viral isolates (**Figure 1–figure supplement 1A**).

Detection of recombinant SARS-CoV-2 protease activity in cells

To test whether these biosensors could detect SARS-CoV-2 protease activity in cells, we co-transfected them with blue fluorescent protein (BFP) plus/minus their cognate SARS-CoV-2 protease into HEK293T cells, and analysed FlipGFP fluorescence after 24 h by flow cytometry (**Figure 1C-F** and **Figure 1–figure supplement 2A**). To control for background FlipGFP fluorescence, mCherry was co-expressed with FlipGFP using a T2A peptide linker, and the ratio of FlipGFP/mCherry fluorescence in BFP+ (transfected) cells used to quantitate reporter activation. Background FlipGFP fluorescence required both parts of the split FlipGFP molecule

bioRxiv preprint doi: https://doi.org/10.1101/2021.03.22.435957; this version posted March 22, 2021. The copyright holder for this preprint (which was not certified by peer review) is the author/funder, who has granted bioRxiv a license to display the preprint in perpetuity. It is made available under aCC-BY 4.0 International license.

(beta-sheets 1-9 and 10/11), and may therefore reflect non-specific cleavage of the FlipGFP oligopeptide linker, or assembly of trimeric complexes, with antiparallel beta-sheets 10 and 11 supplied by separate molecules (**Figure 1–figure supplement 2B**).

Both WT3c-FlipGFP and Opt3c-FlipGFP reporters showed a marked increase in FlipGFP fluorescence in the presence of MPro (**Figure 1C-D**), comparable to the increase seen with the established FlipGFP/TEV protease reporter (**Figure 1–figure supplement 3A-B**). All three PLPro reporters showed an increase in FlipGFP fluorescence in the presence of the PLPro catalytic domain (PLPro c.d.), with the strongest signal from the PLP2-FlipGFP reporter (**Figure 1E-F**). We therefore selected the Opt3c-FlipGFP (MPro) and PLP2-FlipGFP (PLPro) biosensors for further evaluation. To optimise the dynamic range of the flow cytometric assay, we titrated the amount of protease and FlipGFP plasmids, and determined the optimal interval for analysis post-transfection (**Figure 1–figure supplement 2C-E**). We also observed similar results using epifluorescence microscopy (**Figure 1G**).

Confirmation of SARS-CoV-2 protease reporter specificity

To evaluate the specificity of the selected biosensors for their cognate protease, we used the same co-transfection assay in HEK293Ts to measure Opt3c-FlipGFP, PLP2-FlipGFP and TEV-FlipGFP reporter activation in pair-wise combination with MPro, PLPro c.d., or TEV protease (**Figure 1–figure supplement 3A-B**). As a further check, we generated non-cleavable mutants of the Opt3c-FlipGFP and PLP2-FlipGFP reporters. For the Opt3c-FlipGFP reporter, a critical glutamine residue present in the cleavage site was mutated to isoleucine. For the PLP2-FlipGFP reporter, the critical LKGG sequence was scrambled to GLGK. Neither of these non-cleavable mutants showed an increase in FlipGFP fluorescence in the presence of its cognate protease (**Figure 1–figure supplement 3C-F**). Taken together, these results confirm that the selected SARS-CoV-2 biosensors are specific for their cognate proteases, and activated in a strictly sequence-dependent manner.

A cell-based fluorescent assay for inhibitors of MPro activity

bioRxiv preprint doi: https://doi.org/10.1101/2021.03.22.435957; this version posted March 22, 2021. The copyright holder for this preprint (which was not certified by peer review) is the author/funder, who has granted bioRxiv a license to display the preprint in perpetuity. It is made available under aCC-BY 4.0 International license.

To test the utility of FlipGFP-based reporters for screening antiviral compounds in cell-based assays, we focused on the Opt3c-FlipGFP reporter. As positive controls, we first tested GC373 and its pro-drug GC376, which have been reported to inhibit both SARS-CoV and SARS-CoV-2 MPro activity *in vitro*, and viral replication in cells (Kim et al., 2012; Ma et al., 2020; Rathnayake et al., 2020). As expected, a clear dose-dependent decrease in Opt3C-FlipGFP fluorescence was observed in the presence of recombinant MPro and increasing concentrations of either drug (**Figure 2A-C**). Conversely, GC373 did not inhibit PLP2-FlipGFP or TEV-FlipGFP activation by PLPro c.d or TEV protease, respectively (**Figure 2D-G**).

Next, we evaluated a panel of compounds previously reported to have activity against MPro *in vitro*, but which failed to inhibit viral replication in cells (Jin et al., 2020a). In each case, we used the highest concentration tolerated by HEK293Ts for 24 h. Unlike GC373 and GC376, none of these compounds inhibited MPro activity in cells (**Figure 2–figure supplement 1A**). Finally, we tested the HIV-1 protease inhibitors lopinavir and ritonavir (**Figure 2–figure supplement 1B**). These compounds have been reported to have variable activity against MPro activity *in vitro*, but have failed to improve outcomes in clinical trials (Cao et al., 2020; Horby et al., 2020; WHO, 2020). They marginally inhibited MPro activity in cells, but only when used at high doses, sufficient to impact transfection efficiency, reflected by a decreased number of BFP+ cells (**Figure 2–figure supplement 1C**). In summary, these data support the principle that cell-based assays for antiviral compounds correlate better with activity against viral replication than *in vitro* assays.

Activation of FlipGFP-based reporters by wildtype SARS-CoV-2 infection

To test whether our FlipGFP-based reporters could be activated by viral protease expression during SARS-CoV-2 infection, we made use of a permissive HEK293T cell line over-expressing ACE2 (Hoffmann et al., 2020) and furin (Papa et al., 2020), herein termed HEK293T-ACE2 cells. These cells are both readily transfectable with reporter constructs, and demonstrate clear cytopathic effect after 24 h SARS-CoV-2 infection, including the formation of large syncytia (**Figure 3–figure supplement 1A**). Since spike-positive syncytia are lost

bioRxiv preprint doi: https://doi.org/10.1101/2021.03.22.435957; this version posted March 22, 2021. The copyright holder for this preprint (which was not certified by peer review) is the author/funder, who has granted bioRxiv a license to display the preprint in perpetuity. It is made available under aCC-BY 4.0 International license.

during flow cytometric analysis (**Figure 3–figure supplement 1B-C**), we instead used fluorescent microscopy to analyse changes in FlipGFP fluorescence during SARS-CoV-2 infection.

Accordingly, HEK293T-ACE2 cells were plated in chambered coverslips, transfected with the indicated reporter constructs, then infected after 12 h with SARS-CoV-2. After a further 24 h incubation, reporter activation was quantitated as the ratio of FlipGFP/mCherry fluorescence in spike-positive syncytia, compared with uninfected cells. As expected, we observed a consistent increase in FlipGFP fluorescence in infected cells transfected with either the Opt3c-FlipGFP or PLP2-FlipGFP reporter, but not infected cells transfected with non-cleavable controls (**Figure 3A-B**).

Whilst confirming that our FlipGFP reporters could be activated by SARS-CoV-2 infection, the magnitude of effect was, however, markedly reduced compared with the over-expression of recombinant viral proteases (compare **Figure 1D** and **Figure 1F** with **Figure 3B**). This likely reflects lower levels of protease expression during viral infection, compared with over-expression of recombinant proteases (**Figure 3C**). In addition, it is possible that the localisation of proteases and/or presence of other viral proteins and endogenous polyprotein substrates during authentic viral infection reduces their likelihood of encountering reporter molecules. Taken together, these data provided proof-of-concept that protease-activatable biosensors may be exploited to signal SARS-CoV-2 infection, but failed to demonstrate a usable window for high-throughput experiments.

Generation of luciferase-based SARS-CoV-2 protease reporters

To amplify the signal from viral protease expression during SARS-CoV-2 infection, we next developed a luciferase-based system. The 30F-GloSensor reporter comprises an inactive, circularly permuted firefly luciferase (FFluc) molecule (Wigdal et al., 2008). Cleavage of a protease-sensitive oligopeptide linker leads to a conformational change which markedly increases luminescence (**Figure 4A**). Co-expression with Renilla luciferase (Rluc) from the

bioRxiv preprint doi: https://doi.org/10.1101/2021.03.22.435957; this version posted March 22, 2021. The copyright holder for this preprint (which was not certified by peer review) is the author/funder, who has granted bioRxiv a license to display the preprint in perpetuity. It is made available under aCC-BY 4.0 International license.

same vector allows expression levels and cell viability to be normalised between conditions. Similar reporters have previously been used to detect overexpressed MERS-CoV MPro in cell-based assays (Kilianski et al., 2013).

To detect SARS-CoV-2 protease activity, we generated 30F-GloSensor constructs with the same sequence-specific oligopeptide linkers as our FlipGFP-based reporters: 30F-Opt3c, non-cleavable 30F-Opt3c, 30F-PLP2, and non-cleavable 30F-PLP2. Next, we co-transfected them with/without their cognate SARS-CoV-2 protease into HEK293T cells, and analysed FFluc and Rluc luminescence after 24 h (**Figure 4B-C**). As expected, Rluc luminescence was comparable across all conditions, reflecting similar transfection efficiency. Conversely, FFluc luminescence increased dramatically in the presence of cognate SARS-CoV-2 protease. Normalising for Rluc luminescence, we observed a 139-fold increase in luminescence for the 30F-Opt3c/MPro reporter, and a 74-fold increase with the 30F-PLP2/PLPro reporter. Conversely, no increase in signal was seen with the non-cleavable controls. As an additional control, when the reporters were co-transfected pair-wise with non-cognate proteases, no increase in signal was observed (**Figure 4D**).

Quantitation of SARS-CoV-2 infection using luciferase-based reporters

To test whether our luciferase-based reporters could be activated by SARS-CoV-2 infection, we transfected HEK293T-ACE2 cells with the indicated reporter constructs, then infected after 12 h with SARS-CoV-2. After a further 24 h incubation, reporter activation was quantitated as the ratio of FFluc/Rluc luminescence. Compared with uninfected cells, we observed a marked increase in FFluc luminescence in infected cells transfected with either the 30F-Opt3 or 30F-PLP2 reporter, but not infected cells transfected with non-cleavable controls (**Figure 5A-B**). In the context of viral infection, the 30F-PLP2 reporter showed a better dynamic range (29-fold increase in luminescence) than the 30F-Opt3c reporter (9.3-fold increase in luminescence). As expected based on sequence conservation (**Figure 1–figure supplement 1A**), it was also readily activated by recombinant PLPro of SARS-CoV, as well as SARS-CoV-

bioRxiv preprint doi: https://doi.org/10.1101/2021.03.22.435957; this version posted March 22, 2021. The copyright holder for this preprint (which was not certified by peer review) is the author/funder, who has granted bioRxiv a license to display the preprint in perpetuity. It is made available under aCC-BY 4.0 International license.

2 (**Figure 1–figure supplement 1B**). We therefore selected the 30F-PLP2 reporter for further validation in assays for SARS-CoV-2 infection.

To determine how closely the luciferase signal correlated with the number of infected cells, we titrated a SARS-CoV-2 viral stock in HEK293T-ACE2 cells, and measured FFluc and Rluc luminescence in parallel with determining the proportion of spike-positive infected cells using automated microscopy (Cellomics). As expected, the proportion of infected cells increased in accordance with the amount of virus (**Figure 5C-D**). This proportion was mirrored by the luciferase signal (**Figure 5E**), with a correlation coefficient (R2) of 0.93 (**Figure 5F**). Our 30F-PLP2 reporter therefore allows the quantitation of wild-type SARS-CoV-2 replication, using a facile luminescent assay.

A facile luminescent assay for inhibitors of SARS-CoV-2 replication

To test the utility of our luminescent assay for screening candidate antiviral compounds, we transfected HEK293T-ACE2 cells with the 30F-PLP2 reporter 11 h before treatment with remdesivir, GC376, favipiravir, lopinavir or DMSO. After a further 1 h, cells were infected with wildtype SARS-CoV-2 virus and incubated for an additional 24 h before measurement of FFluc and Rluc activities (**Figure 6A**). Similar to published data (Ma et al., 2020; Simonis et al., 2021; Vuong et al., 2020), these experiments allowed us to readily distinguish two antiviral compounds that completely abrogated SARS-COV-2 replication (remdesivir and GC376) from two that did not (favipiravir and lopinavir) (**Figure 6B**). IC_{50} concentrations for remdesivir and GC376 were in the low nanomolar range, corresponding to results from plaque reduction neutralisation tests (PRNT) in other recent studies (Ma et al., 2020; Vuong et al., 2020; Wang et al., 2020). Importantly, since the signal from the 30F-PLP2 reporter was inhibited by remdesivir and GC376, neither of which directly targets PLPro, reporter activation must genuinely reflect viral replication.

A sensitive luminescent reporter cell line for drug, neutralisation and general virological assays

bioRxiv preprint doi: https://doi.org/10.1101/2021.03.22.435957; this version posted March 22, 2021. The copyright holder for this preprint (which was not certified by peer review) is the author/funder, who has granted bioRxiv a license to display the preprint in perpetuity. It is made available under aCC-BY 4.0 International license.

To simplify our assay and adapt it for high-throughput screening, we next generated a stable cell line expressing the 30F-PLP2 luminescent reporter. To achieve this, we re-engineered the 30F-GloSensor plasmid for lentiviral expression by: removing the SV40 poly(A) signal present after the FFluc coding-sequence; replacing the SV40 promoter driving Rluc expression with an internal ribosome entry site (IRES); adding a woodchuck hepatitis virus post-transcriptional regulatory element (WPRE) to increase the expression of the FFluc-IRES-Rluc transcript; and inserting the FFluc-IRES-Rluc-WPRE cassette into a pHSRIN-based lentiviral vector (**Figure 7–figure supplement 1**). We then generated the HEK293T-ACE2-30F-PLP2 reporter cell line by lentiviral transduction of HEK293T-ACE2 cells.

To test this cell line in a scalable format, we seeded HEK293T-ACE2-30F-PLP2 cells in 96-well plates, infected them with wild-type SARS-CoV-2, then measured FFluc and Rluc luminescence after 24 h. As expected, we saw no difference in Rluc signal between mock-infected and SARS-CoV-2-infected cells (**Figure 7A**). Conversely, a dramatic increase in FFluc signal was evident in infected cells, with a 20-fold increase in the FFluc/Rluc ratio (**Figure 7A-B**). Similar to transient expression of the 30F-PLP2 reporter, treatment of the reporter cell line with remdesivir 1 h prior to infection abrogated the increase in luciferase activity (**Figure 7C**). Finally, we used the reporter cells to evaluate the SARS-CoV-2 neutralising activity of two serum samples previously characterised in a spike-pseudotyped lentiviral assay (Mlcochova et al., 2020). As expected, our reporter cell line clearly distinguished convalescent serum from control (non-neutralising) serum, with a sigmoidal titration curve and a neutralising titre at 50% inhibition (NT_{50}) of approximately 1000 (**Figure 7D**). Taken together, these data demonstrate the utility of HEK293T-ACE2-30F-PLP2 cells for drug, neutralisation and general virological assays, using a simple luminescent readout.

bioRxiv preprint doi: https://doi.org/10.1101/2021.03.22.435957; this version posted March 22, 2021. The copyright holder for this preprint (which was not certified by peer review) is the author/funder, who has granted bioRxiv a license to display the preprint in perpetuity. It is made available under aCC-BY 4.0 International license.

Discussion

In this study, we have developed a versatile toolkit of cell-based fluorescent and luminescent reporters activated by SARS-CoV-2 proteases. Our data establish the feasibility of protease-activatable biosensors for the detection of SARS-CoV-2 infection, and demonstrate the practical utility of a luciferase-based reporter cell line for quantification of infected cells, drug testing and serological assays.

SARS-CoV-2 proteases are attractive therapeutic targets, and a feline coronavirus (FCoV) MPro inhibitor has shown promise in treating feline infectious peritonitis (FIP) in cats (Pedersen et al., 2018). FlipGFP-based reporters are ideally suited to the evaluation of small molecule inhibitors of SARS-CoV-2 MPro and/or PLPro activity in cells. In particular, quantification of reporter activation by the ratio of FlipGFP/mCherry fluorescence controls for non-specific changes in cell viability or reporter expression (such as caused by ritonavir and lopinavir). Accordingly, from a panel of inhibitors all previously shown to inhibit MPro *in vitro*, our cell-based assay was able to differentiate between compounds which are able to inhibit viral replication (GC373 and GC376) and those which are not (carmofur, disulfiram, PX-12, tideglusib).

Whilst this manuscript was in preparation, other groups have also described protease-activatable reporters for recombinant SARS-CoV-2 MPro (Drayman et al., 2020; Froggatt et al., 2020; Li et al., 2020; O'Brien et al., 2021; Rawson et al., 2021). In contrast to those studies, our primary aim was to develop practical protease-activatable reporters for authentic viral infection. Whilst we confirmed that FlipGFP-based biosensors may be activated by protease expression during viral infection, we observed a significant compression in their dynamic range in that context, compared with over-expression of recombinant proteases (26-fold to 3-fold for Opt3c/MPro reporter, and 12-fold to 3-fold for PLP2/PLPro reporter). Contributing factors likely include (but may not be limited to): lower protease expression levels plus/minus reduced accessibility during viral infection; background FlipGFP fluorescence; and the absence of

bioRxiv preprint doi: https://doi.org/10.1101/2021.03.22.435957; this version posted March 22, 2021. The copyright holder for this preprint (which was not certified by peer review) is the author/funder, who has granted bioRxiv a license to display the preprint in perpetuity. It is made available under aCC-BY 4.0 International license.

enzymatic signal amplification. Whilst providing proof of concept, FlipGFP-based reporters are therefore unlikely to be used to detect viral replication in practice.

To overcome these limitations, we therefore generated luciferase-based reporters. We envisioned at least three advantages of this approach: first, luciferase-based assays are typically highly sensitive; second, since the first step in measuring luciferase activity involves lysing cells, the readout is not affected by syncytia formation during viral infection; and third, luciferase-based assays may be readily adapted to high-throughput platforms. Accordingly, compared with FlipGFP, the window for luciferase-based reporter activation was greatly increased in assays of recombinant proteases (139-fold versus 26-fold for Opt3c/MPro reporters, and 74-fold versus 12-fold for PLP2/PLPro reporters) and viral infection (12-fold vs. 3-fold for Opt3c/MPro reporters, and 29-fold versus 3-fold for PLP2/PLPro reporters).

Interestingly, whilst our luciferase-based Opt3c/MPro reporter displayed a higher sensitivity for recombinant protease, our PLP2/PLPro reporter performed markedly better during SARS-CoV-2 infection. This may reflect inversion of the expression levels of MPro and PLPro in the different settings, or differential accessibility of the reporters (substrates) to viral proteases in the context of viral infection. Since PLPro of SARS-CoV has deubiquitylation (DUB) activity, and is able to regulate whole cell levels of ubiquitylation during viral infection, we suspect that PLPro of SARS-CoV-2 may also be able to readily access a wide variety of cellular proteins, including cytosolic reporters (Yan and Wu, 2021). Either way, the use of a PLPro (rather than MPro) reporter was critical for the optimisation of our system.

By further reengineering the 30F-PLP2 reporter for lentiviral expression, we have generated the first stable, luminescent reporter cell line for SARS-CoV-2 infection. This simplifies the experimental workflow, and allows facile assays in a 96-well plate format. It is therefore ideally suited to high-throughput screens of candidate antiviral compounds or therapeutic antibodies, and/or large-scale serological surveys for neutralising activity against authentic virus. In fact, whilst the mechanism of reporter activation is different, our HEK293T-ACE2-30F-PLP2 cells are conceptually similar to TZM-bl reporter cells for HIV infection, and we anticipate a similar

bioRxiv preprint doi: https://doi.org/10.1101/2021.03.22.435957; this version posted March 22, 2021. The copyright holder for this preprint (which was not certified by peer review) is the author/funder, who has granted bioRxiv a license to display the preprint in perpetuity. It is made available under aCC-BY 4.0 International license.

range of uses. Further work in our lab is focussed on optimising the assay for a 384-well plate format, and generating stable reporter cell lines in other models of SARS-CoV-2 infection, such as human airway epithelial cells.

Compared with reverse-engineered fluorescent or luminescent reporter viruses, a key advantage of our luminescent reporter cell line is the potential to detect a range of clinical SARS-CoV-2 isolates, including emerging variants of concern. The assessment of the ability of these variants to escape from natural or vaccine-induced immunity has been complicated by variability in the pseudotype assays commonly used by different laboratories (Altmann et al., 2021). Beyond SARS-CoV-2, the PLP2 cleavage sequence is highly conserved in SARS-CoV, and partially conserved in MERS-CoV. This suggests that the Papain-like proteases of these viruses will also be able to activate our 30F-PLP2 biosensor, and we confirmed this in the case of recombinant SARS-CoV PLPro. Our biosensors therefore offer a standardised “off-the-shelf” solution for the quantitation of authentic betacoronavirus replication and neutralisation during this and (potentially) future coronavirus pandemics.

bioRxiv preprint doi: https://doi.org/10.1101/2021.03.22.435957; this version posted March 22, 2021. The copyright holder for this preprint (which was not certified by peer review) is the author/funder, who has granted bioRxiv a license to display the preprint in perpetuity. It is made available under aCC-BY 4.0 International license.

Materials and methods

Key resources table

Reagent type (species) or resource	Designation	Source or reference	Identifiers	Additional information
cell line (human)	HEK293T cells (293Ts)	A kind gift from Paul Lehner	RRID: CVCL_0063	Authenticated by STR profiling (Menzies et al., 2018; Miles et al., 2017)
cell line (human)	HEK293T-ACE2 cells	This paper	Not applicable	See Materials and methods for details
cell line (human)	HEK293T-ACE2-30F-PLP2 cells	This paper	Not applicable	See Materials and methods for details
cell line (monkey)	VeroE6 cells	A kind gift from Rupert Beale	RRID: CVCL_0059	Authenticated by species-specific PCR (IDEXX BioAnalytics)
strain, strain background (SARS-CoV-2)	SARS-CoV-2 virus	A kind gift from Ian Goodfellow	SARS-CoV-2/human/Liverpool/REMRQ0001/2020	See Materials and methods for details
recombinant DNA reagent	PCDNA3-FlipGFP(TEV cleavage seq) T2A mCherry	Addgene	#124429	Encodes FlipGFP (TEV cleavage sequence) and T2A mCherry
recombinant DNA reagent	pcDNA3-FlipGFP beta-sheets 1-9	This paper	Not applicable	See Materials and methods for details
recombinant DNA reagent	pcDNA3-FlipGFP beta-sheets 10/11	This paper	Not applicable	See Materials and methods for details
recombinant DNA reagent	pGloSensor-30F	Promega	Not applicable	Discontinued, but available from Promega upon request
recombinant DNA reagent	pDONR207 SARS-CoV-2 NSP3	Addgene	#141257	Encodes SARS-CoV-2 PLPro
recombinant DNA reagent	pDONR223 SARS-CoV-2 NSP5	Addgene	#141259	Encodes SARS-CoV-2 MPro
recombinant DNA reagent	pHRSIN-30F-PLP2-IRES-hRluc-WPRE-PGK-Puro	This paper	Not applicable	See Materials and methods for details
recombinant DNA reagent	pHRSIN-ACE2-Hygro	This paper	Not applicable	See Materials and methods for details
recombinant DNA reagent	pTAG-BFP-N	Evrogen	FP172	Encodes BFP
recombinant DNA reagent	pcDNA3.1 TEV (full-length)	Addgene	#64276	Encodes TEV protease
recombinant DNA reagent	pHRSIN-Furin-Puro	A kind gift from Paul Lehner	Not applicable	Encodes human furin
recombinant DNA reagent	psPAX2	Addgene	#12260	Lentiviral packaging plasmid
recombinant DNA reagent	pCMV-VSV-G	Addgene	#8454	Lentiviral packaging plasmid
antibody	Anti-NSP3 (743 - 1072) SARS-CoV-2 antibody	MRC PPU reagents	Sheep Number: DA126, 1st bleed	https://mrcppureagents.dundee.ac.uk/reagents-view-antibodies/703270
antibody	Anti-NSP5 SARS-CoV-2 antibody	MRC PPU reagents	Sheep Number: DA118, 2nd bleed	https://mrcppu-covid.bio/antibodies/134216

bioRxiv preprint doi: https://doi.org/10.1101/2021.03.22.435957; this version posted March 22, 2021. The copyright holder for this preprint (which was not certified by peer review) is the author/funder, who has granted bioRxiv a license to display the preprint in perpetuity. It is made available under aCC-BY 4.0 International license.

antibody	Anti-SARS-CoV-2 spike antibody [1A9]	Genetex	GTX632604	For microscopy and flow cytometry (1:500)
antibody	SARS-CoV-2 nucleocapsid antibody	Novus Biologicals	NB100-56683	For immunoblot (1:1000)
antibody	Mouse monoclonal anti-β-actin	Sigma	A5316	For immunoblot (1:20000)
antibody	anti-mouse Alexa Fluor 647 (AF647) secondary antibody	Jackson ImmunoResearch	#715-605-150	For microscopy and flow cytometry (1:1000)
antibody	anti-mouse Alexa Fluor 594 (AF594) secondary antibody	Jackson ImmunoResearch	#715-585-150	For microscopy (1:1000)
commercial assay or kit	Dual-Glo Luciferase Assay System	Promega	E2920	
commercial assay or kit	NEBuilder HiFi DNA Assembly Cloning Kit	NEB	E5520S	
commercial assay or kit	5-alpha Competent *E. coli* (High Efficiency)	NEB	C2987	
commercial assay or kit	Micro BCA Protein Assay Kit	Thermo Fisher	23235	
chemical compound, drug	Lopinavir	APExBIO	A8204	
chemical compound, drug	Ritonavir	APExBIO	A8203	
Chemical compound, drug	PX-12	APExBIO	A4509	
chemical compound, drug	Tideglusib	APExBIO	B1539	
chemical compound, drug	Disulfiram	APExBIO	A4015	
chemical compound, drug	Carmofur	APExBIO	A2548	
chemical compound, drug	GC373	A kind gift from Wayne Vuong, John C. Vederas and M. Joanne Lemieux	Not applicable	(Vuong et al., 2020)
chemical compound, drug	GC376	A kind gift from Wayne Vuong, John C. Vederas and M. Joanne Lemieux	Not applicable	(Vuong et al., 2020)
chemical compound, drug	Remdesivir	APExBIO	B8398	
chemical compound, drug	Favipiravir	BioVision	2778-5	A kind gift from Aartjan te Velthuis
software, algorithm	Prism 8.0	GraphPad	RRID: SCR_002798	
software, algorithm	FlowJo 10.7	TreeStar	RRID: SCR_008520	
software, algorithm	WebLogo	http://weblogo.berkeley.edu	RRID: SCR_010236	(Crooks et al., 2004)

Cell culture

bioRxiv preprint doi: https://doi.org/10.1101/2021.03.22.435957; this version posted March 22, 2021. The copyright holder for this preprint (which was not certified by peer review) is the author/funder, who has granted bioRxiv a license to display the preprint in perpetuity. It is made available under aCC-BY 4.0 International license.

HEK293T cells (a kind gift from Paul Lehner, authenticated by STR profiling (Menzies et al., 2018; Miles et al., 2017)) and VeroE6 cells (a kind gift from Rupert Beale, authenticated by species-specific PCR (IDEXX BioAnalytics)) were cultured in DMEM supplemented with 10% fetal calf serum (FCS), 100 units/ml penicillin, and 0.1 mg/ml streptomycin at 37℃ in 5% CO2. All cells were regularly screened and confirmed to be mycoplasma negative (Lonza MycoAlert and IDEXX BioAnalytics).

Vectors for transgene expression

FlipGFP-based reporters

To generate FlipGFP-based reporters, the TEV FlipGFP plasmid PCDNA3-FlipGFP(TEV cleavage seq) T2A mCherry (Addgene, #124429, a gift from Xiaokun Shu (Zhang et al., 2019)) was used as a template for pairs of PCR reactions including primers designed to generate overlapping products replacing the TEV cleavage site with the indicated cleavage sequence (**Supplementary file 1**). For example, to replace the TEV cleavage site with the PLP2 cleavage sequence, products generated by PCR reactions including 'Near AfeI'/'PLP2 Rv' and 'PLP2 Fw'/'Near AflII' primer pairs were used. The same plasmid was then digested with AfeI and AflII and assembled with the gel purified PCR products using the HiFi Assembly Master Mix (NEB, E5520).

For independent expression of beta sheets 1-9 of FlipGFP, the PCDNA3-FlipGFP (TEV cleavage seq) T2A mCherry plasmid was digested with HindIII and NheI, then assembled with the indicated oligonucleotides (**Supplementary file 1**) as above. For independent expression of beta-sheets 10 and 11 of FlipGFP (including the Opt3c cleavage site), the pcDNA3-Opt3c-FlipGFP plasmid (generated as above) was used as a template for a PCR reaction with the indicated primers (**Supplementary file 1**), then assembled with EcoRI-linearized pcDNA3.1 as above.

Luciferase-based reporters

bioRxiv preprint doi: https://doi.org/10.1101/2021.03.22.435957; this version posted March 22, 2021. The copyright holder for this preprint (which was not certified by peer review) is the author/funder, who has granted bioRxiv a license to display the preprint in perpetuity. It is made available under aCC-BY 4.0 International license.

To generate circularly permuted firefly luciferase (FFluc)-based reporters, the pGloSensor-30F plasmid (Promega) was digested with BamHI and HindIII, then assembled with oligonucleotides encoding the indicated cleavage sequences (**Supplementary file 1**) as above.

To generate a lentiviral expression vector for the 30F-PLP2 reporter, the pCMV-intron-30F-PLP2-pA-pSV40-hRluc reporter cassette was first amplified from the pGloSensor-30F PLP2 plasmid using the indicated primers (**Supplementary file 1**), then assembled with pHRSIN-pCMV-EGFP-PGK-Puro (van den Boomen et al., 2020) digested with EcoRI and NotI as above. Next, the SV40 poly(A) signal and promoter were replaced with an internal ribosome entry site (IRES) to generate the final pHRSIN-30F-PLP2-IRES-hRluc-WPRE-PGK-Puro lentiviral expression vector. In brief, the pA-pSV40-hRluc fragment was excised by digestion with SalI, and replaced by three-way HiFi assembly (as above) with Renilla luciferase amplified by PCR from pGloSensor-30F using the indicated primers (**Supplementary file 1**) and a 586 bp encephalomyocarditis virus (EMCV) IRES sequence. The final sequence of the 30F-PLP2-IRES-hRluc-WPRE-PGK-Puro reporter cassette is shown (**Supplementary file 1**).

<u>Viral proteases</u>

To generate an expression vector for SARS-CoV-2 Main protease (MPro), the open reading frame was amplified by PCR from the pDONR223 SARS-CoV-2 NSP5 plasmid (Addgene, #141259, a gift from Fritz Roth (Kim et al., 2020)), including an ATG start codon in the forward primer and a TAA stop codon in the reverse primer (**Supplementary file 1**), then assembled with EcoRI-linearised pcDNA3.1 as above.

To generate an expression vector for the SARS-CoV-2 Papain-like protease catalytic domain (PLPro c.d.), we used the SARS-CoV nsp3 catalytic domain as a guide (Bekes et al., 2016). The coding sequence from amino acid 747E to 1061K was amplified by PCR from the pDONR207 SARS-CoV-2 NSP3 plasmid (Addgene, #141257, a gift from Fritz Roth (Kim et al., 2020)), including a Kozak sequence and ATG start codon in the forward primer and a TAA

bioRxiv preprint doi: https://doi.org/10.1101/2021.03.22.435957; this version posted March 22, 2021. The copyright holder for this preprint (which was not certified by peer review) is the author/funder, who has granted bioRxiv a license to display the preprint in perpetuity. It is made available under aCC-BY 4.0 International license.

stop codon in the reverse primer (**Supplementary file 1**), then assembled with EcoRI-linearised pcDNA3.1 as above. Where indicated, empty pcDNA3.1 was used as a control.

For expression of TEV protease, pcDNA3.1 TEV (full-length) (Addgene, #64276, a gift from Xiaokun Shu (To et al., 2015)) was used.

To generate an expression vector for the SARS-CoV Papain-like protease catalytic domain (PLPro c.d.) (Bekes et al., 2016), a gene block was synthesized by GenScript (**Supplementary file 1**), then assembled with pcDNA3.1 digested with BamHI and EcoRI as above.

<u>Other transgenes</u>

For expression of BFP, pTAG-BFP-N (Evrogen, FP172) was used.

To generate a lentiviral expression vector for human ACE2, the open reading frame was amplified from a HepG2 cDNA library by PCR using the indicated primers (**Supplementary file 1**), then assembled with pHRSIN-pSFFV-GFP-PGK-Hygro (Tchasovnikarova et al., 2015) digested with KpnI and XhoI to generate pHRSIN-ACE2-Hygro as above.

For expression of human furin, pHRSIN-Furin-Puro (a kind gift from Paul Lehner) was used.

For lentiviral packaging, psPAX2 (Addgene, #12260, a gift from Didier Trono) and pCMV-VSV-G (Addgene, #8454, a gift from Bob Weinberg (Stewart et al., 2003)) were used.

All constructs generated for this study were verified by Sanger sequencing (Source BioScience).

Generation of HEK293T-ACE2 and HEK293T-ACE2-30F-PLP2 cells

For transduction of HEK293T cells with ACE2, a pHRSIN-ACE2-Hygro lentiviral stock was generated by co-transfection of HEK293T cells with psPAX2 and pCMV-VSV-G using standard methods. After selection with hygromycin for 2 weeks, cells were sorted for high cell surface ACE2 expression and single-cell cloned. Following expansion, a clone with stable,

bioRxiv preprint doi: https://doi.org/10.1101/2021.03.22.435957; this version posted March 22, 2021. The copyright holder for this preprint (which was not certified by peer review) is the author/funder, who has granted bioRxiv a license to display the preprint in perpetuity. It is made available under aCC-BY 4.0 International license.

homogeneously high expression of ACE2 (herein termed clone 22) was selected for further experiments. For transduction with furin, a pHRSIN-Furin-Puro lentiviral stock was generated as above, and clone 22 cells (herein termed HEK293T-ACE2 cells) were selected with puromycin for a further 2 weeks. Finally, to generate the HEK293T-ACE2-30F-PLP2 reporter cell line, HEK293T-ACE2 cells were further transduced with a pHRSIN-30F-PLP2-IRES-hRluc-WPRE-PGK-Puro lentiviral stock at MOI=3, generated as above.

Production and titration of SARS-CoV-2 viral stocks

The virus used in this study was the clinical isolate SARS-CoV-2/human/Liverpool/REMRQ0001/2020, a kind gift from Ian Goodfellow (University of Cambridge), isolated by Lance Turtle (University of Liverpool) and David Matthews and Andrew Davidson (University of Bristol) (Daly et al., 2020; Patterson et al., 2020).

Viral stocks were prepared by passaging once in VeroE6 cells. In brief, VeroE6 cells were infected at a low multiplicity of infection (MOI) with the original viral stock, and incubated for 72 h (by which time cytopathic effect was evident). Virus-containing culture supernatants were then clarified by centrifugation at 600 g for 5 mins, and immediately frozen in aliquots at -80°C. Viral stocks were then titrated in VeroE6 cells by 50% tissue culture infectious dose (TCID50) assays using standard methods.

All experiments using SARS-CoV-2 virus were conducted in Containment Level 3 facility of the Jeffrey Cheah Biomedical Centre (JCBC), University of Cambridge.

Flow cytometric analysis of FlipGFP-based reporters in the presence of recombinant proteases

HEK293T cells were seeded at least 12 h in advance and transfected at approximately 50% confluency. Plasmids and TransIT-293 transfection reagent (Mirus) were mixed at a ratio of 1 µg DNA : 3 µLTransit-T293 in Opti-MEM (Gibco). For an experiment conducted in triplicate at a 48-well scale, we typically used (per condition): 150 ng BFP expression vector, 300 ng FlipGFP-based reporter construct, and 450 ng of either empty pcDNA3.1 (control) or

bioRxiv preprint doi: https://doi.org/10.1101/2021.03.22.435957; this version posted March 22, 2021. The copyright holder for this preprint (which was not certified by peer review) is the author/funder, who has granted bioRxiv a license to display the preprint in perpetuity. It is made available under aCC-BY 4.0 International license.

pcDNA3.1 encoding the indicated protease; 2.7 µL TransIT-293; and 150 µL Opti-MEM (for 50 µL of transfection/well).

For titration of SARS-CoV-2 proteases, the total amount of DNA transfected was kept constant by adding additional empty pcDNA3.1. Where indicated, DMSO or candidate inhibitors of recombinant MPro or PLPro were added immediately after transfection.

Unless otherwise indicated, HEK293T cells were dissociated with trypsin 24 h post-transfection, resuspended in PBS + 0.5% FBS and analysed immediately by flow cytometry using a BD LSRFortessa equipped with 405 nm, 488 nm, 561 nm and 640 nm lasers. The ratio of FlipGFP/mCherry mean fluorescence intensity (MFI) in BFP+ (transfected) cells was used to quantitate reporter activation (FlowJo 10.7). An indicative gating strategy is shown in **Figure 1–figure supplement 2A**.

Flow cytometric analysis of spike protein expression in SARS-CoV-2-infected cells

HEK293T-ACE2 cells were seeded at a density of 9 x 10^4 cells/48-well in 250 µL complete media. The following morning, cells were infected with SARS-CoV-2 at MOI=1 and incubated for 24 h.

To measure the fraction of infected cells using flow cytometry, cells were first dissociated with trypsin and fixed for 15 mins by incubation in 4% paraformaldehyde (PFA). Cells were then permeabilised with Perm/Wash buffer (BD), stained for SARS-CoV-2 spike protein using a mouse monoclonal antibody (GeneTex, GTX632604) for 30 mins at room temperature, washed twice, stained with an anti-mouse Alexa Fluor 647 (AF647) secondary antibody (Jackson ImmunoResearch, #715-605-150) for 30 mins at room temperature, washed twice, resuspended in PBS + 0.5% FBS and analysed by flow cytometry as above.

Automated microscopic analysis of spike protein expression in SARS-CoV-2-infected cells

bioRxiv preprint doi: https://doi.org/10.1101/2021.03.22.435957; this version posted March 22, 2021. The copyright holder for this preprint (which was not certified by peer review) is the author/funder, who has granted bioRxiv a license to display the preprint in perpetuity. It is made available under aCC-BY 4.0 International license.

HEK293T-ACE2 cells were seeded at a density 9 x 10^4 cells/well of an 8-well µ-Slide (Ibidi, Cat No 80826) in 250 µL complete media. The following morning, cells were infected with SARS-CoV-2 at MOI=1 and incubated for 24 h.

To measure the fraction of infected cells using automated microscopy, cells were first fixed for 15 mins by incubation in 4% PFA. Cells were then permeabilised with Perm/Wash buffer (BD), stained for SARS-CoV-2 spike protein using a mouse monoclonal antibody (GeneTex, GTX632604) for 30 mins at room temperature, washed twice, stained with an anti-mouse Alexa Fluor 594 (AF594) secondary antibody (Jackson ImmunoResearch, #715-585-150) for 30 mins at room temperature, washed extensively, mounted with 200 µL/well of Fluoroshield Mounting Media (Sigma, F6057), and analysed by automated microscopy.

In brief, images were acquired using a Cellomics ArrayScan XTI high-throughput imaging platform (Thermo Fisher) using a 386 nm excitation/emission filter to detect DAPI-stained nuclei and a 560 nm excitation/emission filter to detect AF594. Images were then analysed with built-in high content HCS Studio software (by Thermo Fisher) using the Target Activation application. For this, cellular objects were identified by applying overlays (masks) based on DAPI intensity. Necessary steps to exclude non-cellular artefacts (large or small objects) were activated based on average nuclei size. Additionally, background correction was performed on both channels. The generated nuclei masks were then applied to the AF594 channel and the threshold for AF594 staining was determined using stained mock-infected cells. Finally, cells were considered infected if their AF594 signal was above this threshold. 42 fields were scanned for each sample/condition to ensure the analysis of a sufficient number of cells.

Confocal microscopic analysis of FlipGFP-based reporters and spike protein expression in SARS-CoV-2-infected cells

HEK293T-ACE2 cells were seeded at a density 9 x 10^4 cells/well of an 8-well µ-Slide (Ibidi, Cat No 80826) in 250 µL complete media. After 1 h, cells were transfected in duplicate with

bioRxiv preprint doi: https://doi.org/10.1101/2021.03.22.435957; this version posted March 22, 2021. The copyright holder for this preprint (which was not certified by peer review) is the author/funder, who has granted bioRxiv a license to display the preprint in perpetuity. It is made available under aCC-BY 4.0 International license.

the indicated FlipGFP-based reporter constructs as above. The following morning, cells were infected with SARS-CoV-2 at MOI=1 and incubated for 24 h.

To measure reporter activation in infected cells using confocal microscopy, cells were first fixed for 15 mins by incubation in 4% PFA. Cells were then permeabilised with Perm/Wash buffer (BD), stained for SARS-CoV-2 spike protein using a mouse monoclonal antibody (GeneTex, GTX632604) for 30 mins at room temperature, washed twice, stained with an anti-mouse AF647 secondary antibody (Jackson ImmunoResearch, #715-605-150) for 30 mins at room temperature, mounted with 200 µL/well of Fluoroshield Mounting Media (Sigma, F6057), and analysed by confocal microscopy using a Zeiss LSM 710 Inverted confocal microscope equipped with 405, 458, 543 and 633 nm lasers and a Plan Apochromat 63X/1.40 Oil DIC M27 objective. For each reporter construct, the ratio of FlipGFP/mCherry MFI was calculated manually using Fiji (ImageJ), by creating a mask around syncytiated cells that were both spike+ (infected) and mCherry+ (transfected).

Immunoblotting

Washed cell pellets were lysed in PBS + 1% Triton supplemented with Halt Protease and Phosphatase Inhibitor Cocktail (Thermo Scientific) for 30 mins on wet ice. Post-nuclear supernatants were heated in Laemelli Loading Buffer for 5 mins at 95℃, separated by SDS-PAGE and transferred to Immobilon-P membrane (Millipore). Membranes were blocked in PBS/5% non-fat dried milk (Marvel)/0.2% Tween and probed with the indicated primary antibody overnight at 4℃. Reactive bands were visualised using HRP-conjugated secondary antibodies and SuperSignal West Pico or Dura chemiluminescent substrates (Thermo Scientific). Typically, 10–20 µg total protein was loaded per lane.

Luminescent analysis of luciferase-based reporters in the presence of recombinant proteases

HEK293T cells were transfected in triplicate at a 48-well scale essentially as for transfection of FlipGFP-based reporter constructs, typically using 150 ng of the indicated pGloSensor-30F

bioRxiv preprint doi: https://doi.org/10.1101/2021.03.22.435957; this version posted March 22, 2021. The copyright holder for this preprint (which was not certified by peer review) is the author/funder, who has granted bioRxiv a license to display the preprint in perpetuity. It is made available under aCC-BY 4.0 International license.

reporter construct and 150 ng of empty pcDNA3.1 (control) or pcDNA3.1 encoding the indicated protease.

After 24 h incubation, media was aspirated from each well, and cells lysed with 50 µL/well Dual-Glo Luciferase Buffer (Promega) diluted 1:1 with PBS + 1% NP-40, for 10 mins at room temperature. Lysates were then transferred to opaque half-area 96-well plates, and reporter activation quantitated as the ratio of firefly luciferase (FFluc)/Renilla luciferase (Rluc) activity measured using the Dual-Glo kit (Promega) according to the manufacturer's instructions. In brief, FFluc activity was first measured using a ClarioStar microplate reader. 25 µL Stop and Glo Buffer and Substrate (Promega) was then added to each well. After incubation for 10 mins at room temperature, Rluc activity was measured using the same ClarioStar microplate reader and the ratio of FFluc/Rluc activity calculated for each condition.

Luminescent analysis of luciferase-based reporters in SARS-CoV-2-infected cells

HEK293T-ACE2 cells were reverse-transfected with plasmids and TransIT-293 at a ratio of 1 µg DNA : 3 µLTransit-T293 in Opti-MEM (Gibco). For an experiment conducted in triplicate at a 48-well scale, we typically used (per condition): 900 ng pGloSensor-30F reporter construct; 2.7 µL TransIT-293; and 150 µL Opti-MEM (for 50 µL of transfection mix/well). 2.7 x 10^5 cells were dissociated with Accutase, combined with the transfection mix, and seeded at 9 x 10^4 cells/well.

The following morning, cells were infected with SARS-CoV-2 at MOI=1 (or for the titration experiments, with the indicated volume of viral stock) and incubated for 24 h. Media was aspirated from each well, and cells lysed with 50 µL/well of Dual-Glo Luciferase Buffer (Promega) diluted 1:1 with PBS + 1% NP-40 for 10 mins at room temperature. Lysates were then transferred to opaque half-area 96-well plates, and reporter activation quantitated as the ratio of FFluc/Rluc activity as above. Where indicated, candidate antivirals were added to the cells 1 h before infection with SARS-CoV-2.

Luminescent analysis of SARS-CoV-2-infected HEK293T-ACE2-30F-PLP2 reporter cells

bioRxiv preprint doi: https://doi.org/10.1101/2021.03.22.435957; this version posted March 22, 2021. The copyright holder for this preprint (which was not certified by peer review) is the author/funder, who has granted bioRxiv a license to display the preprint in perpetuity. It is made available under aCC-BY 4.0 International license.

HEK293T-ACE2-30F-PLP2 reporter cells were seeded at a density of 4 x 10^4 cells/96-well in 100 µL complete media. The following morning, cells were infected with SARS-CoV-2 at MOI=1 and incubated for 24 h. Media was aspirated from each well, and cells lysed with 25 µL/well of Dual-Glo Luciferase Buffer (Promega) diluted 1:1 with PBS + 1% NP-40 for 10 mins at room temperature. Lysates were then transferred to opaque half-area 96-well plates, and reporter activation quantitated as the ratio of FFluc/Rluc activity as above. For evaluation of candidate antivirals, compounds were added to the cells 1 hr before infection with SARS-CoV-2. To measure SARS-CoV-2 neutralising activity, SARS-CoV-2 viral stock was pre-incubated with serial dilutions of heat-inactivated sera (a kind gift from Ravi Gupta) for 2 h at 37°C, prior to addition to the cells.

SARS-CoV-2, SARS-CoV, and MERS-CoV sequence logos

A SARS-CoV-2 genomic alignment file was retrieved from the GISAID database (https://www.epicov.org/). At the time of access (30/06/2020), this alignment (msa_0630) contained 50,387 sequences. Genome sequences and alignments for MERS-CoV and SARS-CoV were accessed via the NCBI Virus portal (https://www.ncbi.nlm.nih.gov/labs/virus/vssi/#/virus?SeqType_s=Nucleotide). For the MERS-CoV sequences, we searched the database for Virus with taxonid=1335626 and Host with taxonid='human'. We set the nucleotide completeness option to 'complete' and alignments were generated using the NCBI alignment function. Consensus sequences automatically generated and included in the alignment file where removed. For the SARS-CoV sequences, we searched the database for Virus with taxonid=694009 and Host taxonid= 'human'. Because of the large number of sequences (~15,000), it was not possible to perform the alignment using the NCBI alignment function. Instead, FASTA sequences were downloaded and aligned using MAFFT (Katoh et al., 2002) with default parameters.

Having manually inspected the genomic alignments to identify the regions of interest, we used the 'extractalign' function in the European Molecular Biology Open Software Suite (EMBOSS) (Rice et al., 2000). In the case of the GISAID alignment, we removed entries that were

bioRxiv preprint doi: https://doi.org/10.1101/2021.03.22.435957; this version posted March 22, 2021. The copyright holder for this preprint (which was not certified by peer review) is the author/funder, who has granted bioRxiv a license to display the preprint in perpetuity. It is made available under aCC-BY 4.0 International license.

incomplete or that presented nucleotide ambiguities (non-CTGA bases). The resulting sets (one per region of interest and four per alignment inspected) were conceptually translated using the 'transeq' function in EMBOSS. The resulting amino acid sequences were used as input for the WebLogo application (Crooks et al., 2004; Schneider and Stephens, 1990).

Statistical analysis

General data manipulation was conducted using Microsoft Excel, and statistical analysis using Graphpad Prism. Unless otherwise stated, sample means were compared by one-way ANOVA followed by Tukey's multiple comparison test. To calculate half-maximal inhibitory concentrations (IC50s), FFluc/Rluc ratios were analysed using the log(inhibitor) vs. response -- Variable slope (four parameters) function. To calculate neutralising antibody titres at 50% inhibition (NT50s), FFluc/Rluc ratios were analysed using the Sigmoidal, 4PL, X is log(concentration) function.

bioRxiv preprint doi: https://doi.org/10.1101/2021.03.22.435957; this version posted March 22, 2021. The copyright holder for this preprint (which was not certified by peer review) is the author/funder, who has granted bioRxiv a license to display the preprint in perpetuity. It is made available under aCC-BY 4.0 International license.

Acknowledgements

This work was supported by the MRC (CSF ref. MR/P008801/1 to NJM), NHSBT (grant ref. WPA15-02 to NJM), Addenbrooke's Charitable Trust (grant ref. to 900239 NJM), the Rosetree Trust (grant ref. G103718 to JRZ) and the NIHR Cambridge BRC. The authors thank Mark Wills for overseeing the Containment Level 3 facility, Nika Romashova for assistance with automated microscopy, Paul Lehner, James Nathan, Wayne Vuong, John C. Vederas, M. Joanne Lemieux, Aartjan te Velthuis, Rupert Beale, Ian Goodfellow and Ravi Gupta for supplying key reagents, and members of the Matheson and Lehner laboratories for critical discussion.

Competing interests

The authors declare no competing interests.

bioRxiv preprint doi: https://doi.org/10.1101/2021.03.22.435957; this version posted March 22, 2021. The copyright holder for this preprint (which was not certified by peer review) is the author/funder, who has granted bioRxiv a license to display the preprint in perpetuity. It is made available under aCC-BY 4.0 International license.

Figures

Figure 1. FlipGFP-based SARS-CoV-2 protease reporters

(A) Diagram of FlipGFP-based reporter containing the Opt3c protease cleavage sequence (TVRLQSGF). After cleavage by SARS-CoV-2 MPro, GFP beta-sheets 10 and 11 adopt an anti-parallel conformation and self-assemble with beta-sheets 1-9, restoring GFP fluorescence. Adapted from Zhang et al., 2019 (Zhang et al., 2019).

(B) Diagram of pp1a polyprotein showing candidate SARS-CoV-2 cleavage sequences. Three sequences for PLPro (PLP1, PLP2 and PLP3) and one sequence for MPro (WT3c) were chosen. Sites of cleavage are highlighted in red (C-terminal side of indicated amino acid).

(C-F) Activation of FlipGFP-based reporters by recombinant SARS-CoV-2 protease expression. HEK293T cells were co-transfected with FlipGFP-based reporter constructs encoding candidate MPro (WT3c or Opt3C, C-D) or PLPro (PLP1-3, E-F) cleavage sequences, BFP and either MPro (C-D) or PLPro (E-F), or empty pcDNA3.1 as a control. For FlipGFP and mCherry fluorescence in BFP+ cells were analysed by flow cytometry 24 h post-transfection (**Figure 1–figure supplement 2A**). Illustrative flow cytometry data and mean values ± SEM are shown for an experiment performed in triplicate. **** $p<0.0001$. Representative of 5 independent experiments.

(G) Detection of FlipGFP-based reporter activation by epifluorescence microscopy. HEK293T cells were co-transfected with Opt3c-FlipGFP biosensor plus/minus MPro (left panel) or PLP2-FlipGFP biosensor plus/minus PLPro (right panel). FlipGFP and mCherry fluorescence were analysed by epifluorescence microscopy 24 h post-transfection. mCherry, red. FlipGFP, green. Representative of 3 independent experiments.

MPro, recombinant SARS-CoV-2 Main Protease. PLPro c.d., catalytic domain of recombinant SARS-CoV-2 Papain-Like Protease.

Figure 2. Evaluation of candidate SARS-CoV-2 protease inhibitors

bioRxiv preprint doi: https://doi.org/10.1101/2021.03.22.435957; this version posted March 22, 2021. The copyright holder for this preprint (which was not certified by peer review) is the author/funder, who has granted bioRxiv a license to display the preprint in perpetuity. It is made available under aCC-BY 4.0 International license.

(A-B) Inhibition of MPro-dependent Opt3c-FlipGFP biosensor activation by GC373 and GC376. HEK293T cells were co-transfected with Opt3c-FlipGFP biosensor and BFP plus/minus MPro, then treated with DMSO, GC373 (100 µM) or GC376 (100 µM). FlipGFP and mCherry fluorescence in BFP+ cells were analysed by flow cytometry 24 h post-transfection. Illustrative flow cytometry data and mean values ± SEM are shown for an experiment performed in triplicate. **** $p<0.0001$. Representative of 3 independent experiments.

(C) Dose responses to GC373 and GC376. HEK293T cells were co-transfected with Opt3c-FlipGFP biosensor, BFP and MPro, then treated with DMSO or decreasing doses of GC373 or GC373 (100, 25, 6.25, and 1.56 µM). FlipGFP and mCherry fluorescence in BFP+ cells were analysed by flow cytometry 24 h post-transfection. Illustrative flow cytometry data and mean values ± SEM are shown for an experiment performed in triplicate. Representative of 2 independent experiments.

(D-G) Specificity of GC376. HEK293T cells were co-transfected with PLP2-FlipGFP biosensor and BFP plus/minus PLPro (D-E) or TEV-FlipGFP and BFP plus/minus TEV protease (F-G), then treated with DMSO or GC376 (100 µM). FlipGFP and mCherry fluorescence in BFP+ cells were analysed by flow cytometry 24 h post-transfection. Illustrative flow cytometry data and mean values ± SEM are shown for an experiment performed in triplicate. Representative of 2 independent experiments.

MPro, recombinant SARS-CoV-2 Main Protease. PLPro c.d., catalytic domain of recombinant SARS-CoV-2 Papain-Like Protease. TEV, recombinant TEV protease.

Figure 3. FlipGFP-based biosensors of SARS-CoV-2 infection

(A-B) Activation of FlipGFP-based reporters by SARS-CoV-2 infection. HEK293T-ACE2 cells were transfected with Opt3c-FlipGFP, non-cleavable Opt3c-FlipGFP, PLP2-FlipGFP, or non-cleavable PLP2-FlipGFP biosensors, incubated for 12 h, then infected with SARS-CoV-2 at MOI=1. Cells were fixed, permeabilised and stained for SARS-CoV-2 spike protein 24 h post-

bioRxiv preprint doi: https://doi.org/10.1101/2021.03.22.435957; this version posted March 22, 2021. The copyright holder for this preprint (which was not certified by peer review) is the author/funder, who has granted bioRxiv a license to display the preprint in perpetuity. It is made available under aCC-BY 4.0 International license.

infection. FlipGFP and mCherry fluorescence in spike+ syncytia versus spike- cells were analysed by confocal microscopy. Illustrative microscopy data (A) and mean values ± SEM are shown for at least 15 syncytia/cells from each condition (B). **** p<0.0001. mCherry, red. FlipGFP, green. Spike, yellow. DAPI, blue. DIC, differential interference contrast. Representative of 2 independent experiments.

(C) Expression levels of SARS-CoV-2 proteases. HEK293T-ACE2 cells were mock-infected, infected with SARS-CoV-2 at MOI=1 or transfected with MPro (left panel) or PLPro (right panel) under standard conditions. Cells were lysed after 24 h and analysed by immunoblot using antibodies specific for nsp5 (MPro), the PLPro c.d. of nsp3 or nucleocapsid. β-actin was included as a loading control. Arrows indicate presumed full-length nsp3 (215 kDa) and intermediate cleavage products present in SARS-CoV-2 infected cells. Asterisk indicates recombinant PLPro c.d.. Representative of 2 independent experiments.

O.E., over-expression. MPro, recombinant SARS-CoV-2 Main Protease. PLPro c.d., catalytic domain of recombinant SARS-CoV-2 Papain-Like Protease.

Figure 4. Luciferase-based SARS-CoV-2 proteases reporters

(A) Diagram of 30F-GloSensor luciferase-based reporter containing the Opt3c cleavage sequence (TVRLQSGF). Cleavage by SARS-CoV-2 MPro leads to a conformational change in the circularly permuted firefly luciferase (FFluc) molecule, markedly increasing luminescence. 30-FF-358-544/30-FF-4-354, circularly permuted firefly luciferase-based reporter (numbers indicate positions of amino acids in wildtype FFluc). Adapted from Wigdal et al. (Wigdal et al., 2008).

(B-C) Activation of luciferase-based reporters by recombinant SARS-CoV-2 protease expression. HEK293T cells were co-transfected with 30F-Opt3c, non-cleavable 30F-Opt3c, 30F-PLP2, or non-cleavable 30F-PLP2 biosensors plus/minus MPro or PLPro, and FFluc and Renilla luciferase (Rluc) activities measured by luminometry 24 h post-transfection. Mean FFluc and Rluc luminescence and FFluc/Rluc ratios ± SEM are shown for a representative

bioRxiv preprint doi: https://doi.org/10.1101/2021.03.22.435957; this version posted March 22, 2021. The copyright holder for this preprint (which was not certified by peer review) is the author/funder, who has granted bioRxiv a license to display the preprint in perpetuity. It is made available under aCC-BY 4.0 International license.

experiment performed in triplicate (B). Mean fold-changes in FFluc/Rluc ratios ± SEM in the presence or absence of cognate protease are shown for 3 independent experiments, each performed in triplicate (C). **** p<0.0001. RLU, relative light units.

(D) Specificity of luciferase-based reporters. HEK293T cells were co-transfected with 30F-Opt3c or 30F-PLP2 biosensors plus/minus MPro, PLPro or TEV proteases, and FFluc and Rluc activities measured by luminometry 24 h post-transfection. Mean FFluc and Rluc luminescence and FFluc/Rluc ratios ± SEM are shown for an experiment performed in triplicate. Representative of 2 independent experiments.

MPro, recombinant SARS-CoV-2 Main Protease. PLPro c.d., catalytic domain of recombinant SARS-CoV-2 Papain-Like Protease. TEV, recombinant TEV protease.

Figure 5. Luciferase-based biosensors of SARS-CoV-2 infection

(A-B) Activation of luciferase-based reporters by SARS-CoV-2 infection. HEK293T-ACE2 cells were transfected with 30F-Opt3c, non-cleavable 30F-Opt3c, 30F-PLP2, or non-cleavable 30F-PLP2 biosensors, incubated for 12 h, then infected with SARS-CoV-2 at MOI=1. FFluc and Rluc activities were measured by luminometry 24 h post-infection. Mean FFluc and Rluc luminescence and FFluc/Rluc ratios ± SEM are shown for a representative experiment performed in triplicate (A). Mean fold-changes in FFluc/Rluc ratios ± SEM in the presence or absence of SARS-CoV-2 infection are shown for 3 independent experiments, each performed in triplicate (B). *** p<0.001, **** p<0.0001. RLU, relative light units.

(C-F) Quantitation of infected cells. HEK293T-ACE2 cells were transfected with 30F-PLP2 biosensor, incubated for 12 h, then mock-infected or infected with increasing doses of SARS-CoV-2. Cells were analysed in parallel 24 h post-infection by either epifluorescence microscopy for SARS-CoV-2 spike protein (C-D), or luminometry for FFluc and Rluc activities (E). Spike+ cells were enumerated by automated microscopy (Cellomics). Illustrative microscopy data (C) and mean values ± SEM (D-E) are shown for an experiment performed in duplicate (microscopy) or triplicate (luminometry). The correlation between FFluc/Rluc ratios

bioRxiv preprint doi: https://doi.org/10.1101/2021.03.22.435957; this version posted March 22, 2021. The copyright holder for this preprint (which was not certified by peer review) is the author/funder, who has granted bioRxiv a license to display the preprint in perpetuity. It is made available under aCC-BY 4.0 International license.

and the proportions of spike+ cells is shown (F). Spike, red. DAPI, blue. DIC, differential interference contrast. Representative of 2 independent experiments.

Figure 6. Evaluation of candidate SARS-CoV2 antivirals

(A) Schematic of experiment to evaluate candidate antivirals using 30F-PLP2 biosensor.

(B) Inhibition of SARS-CoV-2 replication by candidate antivirals. HEK293T-ACE2 cells were transfected with 30F-PLP2 biosensor, incubated for 12 h, then infected with SARS-CoV-2 at MOI=1. From 1 h prior to infection, cells were treated with DMSO or decreasing doses of antivirals. FFluc and Rluc activities were measured by luminometry 24 h post-infection. Mean FFluc/Rluc ratios ± SEM are shown (as % DMSO-treated cells) for an experiment performed in triplicate. Titration curves and IC50s are included for remdesivir and GC376. Representative of 2 independent experiments.

Figure 7. Luminescent SARS-CoV-2 reporter cell line

(A-B) Activation of reporter cells by SARS-CoV-2 infection. HEK293T-ACE2-30F-PLP2 cells were infected with SARS-CoV-2 at MOI=1. FFluc and Rluc activities were measured by luminometry 24 h post-infection. Mean FFluc and Rluc luminescence and FFluc/Rluc ratios (A) and fold-change in FFluc/Rluc ratio (B) ± SEM are shown for an experiment performed in triplicate. Representative of 3 independent experiments. RLU, relative light units.

(C) Inhibition of SARS-CoV-2 infection by remdesivir. HEK293T-ACE2-30F-PLP2 cells were infected with SARS-CoV-2 at MOI=1. From 1 h prior to infection, cells were treated with DMSO or remdesivir. FFluc and Rluc activities were measured by luminometry 24 h post-infection. Mean FFluc/Rluc ratios ± SEM are shown (as % DMSO-treated cells) for an experiment performed in triplicate. Representative of 2 independent experiments.

(D) SARS-CoV2 neutralisation assay. HEK293T-ACE2-30F-PLP2 cells were infected with SARS-CoV-2 at MOI=1 following pre-incubation with serial dilutions of control or convalescent serum for 2 h at 37°C. FFluc and Rluc activities were measured by luminometry 24 h post-

bioRxiv preprint doi: https://doi.org/10.1101/2021.03.22.435957; this version posted March 22, 2021. The copyright holder for this preprint (which was not certified by peer review) is the author/funder, who has granted bioRxiv a license to display the preprint in perpetuity. It is made available under aCC-BY 4.0 International license.

infection. Mean FFluc/Rluc ratios ± SEM are shown (as % cells treated with SARS-CoV-2 at MOI=1 without pre-incubation with serum) for an experiment performed in triplicate. Representative of 2 independent experiments.

bioRxiv preprint doi: https://doi.org/10.1101/2021.03.22.435957; this version posted March 22, 2021. The copyright holder for this preprint (which was not certified by peer review) is the author/funder, who has granted bioRxiv a license to display the preprint in perpetuity. It is made available under aCC-BY 4.0 International license.

Figure supplements

Figure 1–figure supplement 1. Cleavage sequences of other highly pathogenic human betacoronaviruses

(A) Conservation of cleavage sequences. Amino acid sequence logos for cleavage sequences between nsp1/nsp2 (PLP1), nsp2/nsp3 (PLP2), nsp3/nsp4 (PLP3), and nsp4/nsp5 (WT3c) of SARS-CoV-2, SARS-CoV and MERS-CoV viruses. Relative letter heights indicate conservation across the sequences analysed.

(B) FlipGFP-based reporter activation by PLPro of SARS-CoV. HEK293T cells were co-transfected with 30F-PLP2 biosensor and PLPro of either SARS-CoV-2 or SARS-CoV, and FFluc and Rluc activities measured by luminometry 24 h post-transfection. Mean fold-changes in FFluc/Rluc ratios ± SEM in the presence or absence of protease are shown for an experiment performed in triplicate. Representative of 2 independent experiments.

PLPro c.d., catalytic domain of recombinant Papain-Like Protease.

Figure 1–figure supplement 2. Optimisation of FlipGFP-based reporters

(A) Indicative gating strategy for flow cytometry experiments using FlipGFP-based reporters. Cells were typically gated on FSC-H and SSC-H, and doublets excluded using FSC-W. FlipGFP and mCherry fluorescence were analysed in BFP+ (transfected) cells. Data illustrate change in fluorescence of Opt3c-FlipGFP biosensor in the presence (lower panels) or absence (upper panels) of MPro.

(B) Origin of background FlipGFP fluorescence. HEK293T cells were transfected with BFP and GFP1-9-T2A-mCherry (encoding FlipGFP beta-sheets 1-9), GFP10-E5-GFP11-Opt3c-K5 (encoding FlipGFP beta-sheets 10-11) or Opt3c-FlipGFP biosensor plus/minus MPro. FlipGFP and mCherry fluorescence in BFP+ cells were analysed by flow cytometry 24 h post-transfection. Representative of 2 independent experiments.

bioRxiv preprint doi: https://doi.org/10.1101/2021.03.22.435957; this version posted March 22, 2021. The copyright holder for this preprint (which was not certified by peer review) is the author/funder, who has granted bioRxiv a license to display the preprint in perpetuity. It is made available under aCC-BY 4.0 International license.

(C-D) Optimisation of FlipGFP-based reporter/protease ratio. HEK239T cells were co-transfected with BFP and increasing amounts of Opt3c-FlipGFP biosensor plus/minus MPro, keeping the total amount of plasmid DNA constant by adding empty pcDNA3.1. FlipGFP and mCherry fluorescence in BFP+ cells were analysed by flow cytometry 24 h post-transfection. Illustrative flow cytometry data and mean values ± SEM are shown for an experiment performed in duplicate. Representative of 2 independent experiments.

(E) Optimisation of interval between transfection and analysis. HEK293T cells were transfected Opt3c-FlipGFP biosensor, BFP plus/minus MPro. FlipGFP and mCherry fluorescence in BFP+ cells were analysed by flow cytometry 24 h or 36 h post-transfection. Illustrative flow cytometry data and mean values ± SEM are shown for an experiment performed in duplicate. Representative of 2 independent experiments.

MPro, recombinant SARS-CoV-2 Main Protease.

Figure 1–figure supplement 3. Specificity of FlipGFP-based reporters

(A-B) Specificity of FlipGFP-based reporters for cognate proteases. HEK293T cells were co-transfected with Opt3c-FlipGFP, PLP2-FlipGFP, and TEV-FlipGFP biosensors, BFP and MPro, PLPro c.d., or TEV protease. FlipGFP and mCherry fluorescence in BFP+ cells were analysed by flow cytometry 24 h post-transfection. Illustrative flow cytometry data (A) and mean values ± SEM (B) are shown for an experiment performed in triplicate. **** $p<0.0001$. Representative of 3 independent experiments.

(C-D) Sequence specificity of MPro. HEK293T cells were co-transfected with Opt3c-FlipGFP or non-cleavable Opt3c-FlipGFP biosensors, BFP plus/minus MPro. FlipGFP and mCherry fluorescence in BFP+ cells were analysed by flow cytometry 24 h post-transfection. Illustrative flow cytometry data (C) and mean values ± SEM (D) are shown for an experiment performed in triplicate. **** $p<0.0001$. Cleavable/non-cleavable Opt3c sequences are shown, with the cleavage site highlighted in red (C-terminal side of the indicated amino acid). Representative of 3 independent experiments.

bioRxiv preprint doi: https://doi.org/10.1101/2021.03.22.435957; this version posted March 22, 2021. The copyright holder for this preprint (which was not certified by peer review) is the author/funder, who has granted bioRxiv a license to display the preprint in perpetuity. It is made available under aCC-BY 4.0 International license.

(E-F) Sequence specificity of PLPro. HEK293T cells were co-transfected with PLP2-FlipGFP or non-cleavable PLP2-FlipGFP biosensors, BFP plus/minus PLPro. FlipGFP and mCherry fluorescence in BFP+ cells were analysed by flow cytometry 24 h post-transfection. Illustrative flow cytometry data (E) and mean values ± SEM (F) are shown for an experiment performed in triplicate. **** $p<0.0001$. Cleavable/non-cleavable PLP2 sequences are shown, with the cleavage site highlighted in red (C-terminal side of the indicated amino acid). Representative of 3 independent experiments.

MPro, recombinant SARS-CoV-2 Main Protease. PLPro c.d., catalytic domain of recombinant SARS-CoV-2 Papain-Like Protease. TEV, recombinant TEV protease.

Figure 2–figure supplement 1. Evaluation of additional SARS-CoV-2 protease inhibitors

(A) MPro-dependent Opt3c-FlipGFP biosensor activation in the presence of candidate protease inhibitors. HEK293T cells were co-transfected with Opt3c-FlipGFP biosensor, BFP plus/minus MPro, then treated with DMSO or protease inhibitors. FlipGFP and mCherry fluorescence in BFP+ cells were analysed by flow cytometry 24 h post-transfection. Mean values ± SEM are shown for an experiment performed in duplicate. Representative of 2 independent experiments.

(B) Dose responses to lopinavir and ritonavir. HEK293T cells were co-transfected with Opt3c-FlipGFP biosensor, BFP plus/minus MPro, then treated with DMSO or decreasing doses of lopinavir or ritonavir (25, 12, 6 and 3 µM). 24 h post-transfection cells were analysed by FACS. FlipGFP and mCherry fluorescence in BFP+ cells were analysed by flow cytometry 24 h post-transfection. Mean values ± SEM are shown for an experiment performed in duplicate. Representative of 2 independent experiments.

(C) Effects of GC373, GC376, lopinavir and ritonavir on transfection efficiency. The proportion of BFP+ (transfected) cells was analysed by flow cytometry for cells from (B) for lopinavir and ritonavir, and from **Figure 2C** for GC373 and GC376. Mean values +/- SEM are shown for an experiment performed in duplicate. Representative of 2 independent experiments.

bioRxiv preprint doi: https://doi.org/10.1101/2021.03.22.435957; this version posted March 22, 2021. The copyright holder for this preprint (which was not certified by peer review) is the author/funder, who has granted bioRxiv a license to display the preprint in perpetuity. It is made available under aCC-BY 4.0 International license.

Figure 3–figure supplement 1. Infection of HEK293T-ACE2 cells by SARS-CoV-2

(A) Cytopathic effect in HEK293T-ACE2 cells. HEK293T or HEK293T-ACE2 cells were infected with SARS-CoV-2 at MOI=1 then examined for cytopathic effect using brightfield microscopy after 24 h. Representative of >10 independent experiments.

(B-C) Loss of spike+ HEK293T-ACE2 cells during flow cytometric analysis. HEK293T-ACE2 cells were infected with SARS-CoV-2 at MOI=1. Cells were analysed in parallel 24 h post-infection for SARS-CoV-2 spike protein by either automated microscopy (Cellomics) or flow cytometry. In each case, the proportion of spike+ cells was measured. Illustrative data (B) and mean values ± SEM (C) are shown for an experiment performed in triplicate. **** $p<0.0001$. Spike, yellow. DAPI, blue. Representative of 2 independent experiments.

Figure 7–figure supplement 1. 30F-PLP2 constructs

Diagrams of 30F-PLP2 luciferase-based reporter in pGloSensor-30F and pHRSIN-30F-PLP2-IRES-hRluc-WPRE-PGK-Puro expression vectors. 30-FF-358-544/30-FF-4-354, circularly permuted firefly luciferase-based reporter, orange (numbers indicate positions of amino acids in wildtype FFluc). hRluc, codon-optimised (humanised) Renilla luciferase, cyan. LTR, HIV-1 long terminal repeat, yellow. IRES, internal ribosome entry site, brown. WPRE, woodchuck hepatitis virus post-transcriptional regulatory element (WPRE), purple. PuroR, puromycin resistance, green.

bioRxiv preprint doi: https://doi.org/10.1101/2021.03.22.435957; this version posted March 22, 2021. The copyright holder for this preprint (which was not certified by peer review) is the author/funder, who has granted bioRxiv a license to display the preprint in perpetuity. It is made available under aCC-BY 4.0 International license.

Supplementary files

Supplementary file 1. Sequences of PCR primers, oligonucleotides and constructs used in this study

bioRxiv preprint doi: https://doi.org/10.1101/2021.03.22.435957; this version posted March 22, 2021. The copyright holder for this preprint (which was not certified by peer review) is the author/funder, who has granted bioRxiv a license to display the preprint in perpetuity. It is made available under aCC-BY 4.0 International license.

References

Altmann, D.M., Boyton, R.J., and Beale, R. (2021). Immunity to SARS-CoV-2 variants of concern. Science *371*, 1103-1104.

An, W.F., and Tolliday, N. (2010). Cell-based assays for high-throughput screening. Mol Biotechnol *45*, 180-186.

Arias-Arias, J.L., MacPherson, D.J., Hill, M.E., Hardy, J.A., and Mora-Rodriguez, R. (2020). A fluorescence-activatable reporter of flavivirus NS2B-NS3 protease activity enables live imaging of infection in single cells and viral plaques. J Biol Chem *295*, 2212-2226.

Bekes, M., van der Heden van Noort, G.J., Ekkebus, R., Ovaa, H., Huang, T.T., and Lima, C.D. (2016). Recognition of Lys48-Linked Di-ubiquitin and Deubiquitinating Activities of the SARS Coronavirus Papain-like Protease. Mol Cell *62*, 572-585.

Cao, B., Wang, Y., Wen, D., Liu, W., Wang, J., Fan, G., Ruan, L., Song, B., Cai, Y., Wei, M.*, et al.* (2020). A Trial of Lopinavir–Ritonavir in Adults Hospitalized with Severe Covid-19. New England Journal of Medicine *382*, 1787-1799.

Chen, Y., Liu, Q., and Guo, D. (2020). Emerging coronaviruses: Genome structure, replication, and pathogenesis. J Med Virol *92*, 418-423.

Chuck, C.P., Chong, L.T., Chen, C., Chow, H.F., Wan, D.C., and Wong, K.B. (2010). Profiling of substrate specificity of SARS-CoV 3CL. PLoS One *5*, e13197.

Crooks, G.E., Hon, G., Chandonia, J.M., and Brenner, S.E. (2004). WebLogo: a sequence logo generator. Genome Res *14*, 1188-1190.

Daly, J.L., Simonetti, B., Klein, K., Chen, K.E., Williamson, M.K., Anton-Plagaro, C., Shoemark, D.K., Simon-Gracia, L., Bauer, M., Hollandi, R.*, et al.* (2020). Neuropilin-1 is a host factor for SARS-CoV-2 infection. Science *370*, 861-865.

Donal, T.S., Adam, C.H., Javier, G.-J., Michael, L.K., Stephanie, L., Anthony, B., Sandra, A., Emily, A., Helen, B., Medawar Laboratory, T.*, et al.* (2021). Research Square.

Drayman, N., Jones, K.A., Azizi, S.-A., Froggatt, H.M., Tan, K., Maltseva, N.I., Chen, S., Nicolaescu, V., Dvorkin, S., Furlong, K.*, et al.* (2020). Drug repurposing screen identifies

bioRxiv preprint doi: https://doi.org/10.1101/2021.03.22.435957; this version posted March 22, 2021. The copyright holder for this preprint (which was not certified by peer review) is the author/funder, who has granted bioRxiv a license to display the preprint in perpetuity. It is made available under aCC-BY 4.0 International license.

masitinib as a 3CLpro inhibitor that blocks replication of SARS-CoV-2 <em>in vitro</em&gt. bioRxiv, 2020.2008.2031.274639.

Froggatt, H.M., Heaton, B.E., and Heaton, N.S. (2020). Development of a Fluorescence-Based, High-Throughput SARS-CoV-2 3CL(pro) Reporter Assay. J Virol *94*.

Harrington, D.P., Baden, L.R., and Hogan, J.W. (2021). A Large, Simple Trial Leading to Complex Questions. N Engl J Med *384*, 576-577.

Hoffmann, M., Kleine-Weber, H., Schroeder, S., Kruger, N., Herrler, T., Erichsen, S., Schiergens, T.S., Herrler, G., Wu, N.H., Nitsche, A.*, et al.* (2020). SARS-CoV-2 Cell Entry Depends on ACE2 and TMPRSS2 and Is Blocked by a Clinically Proven Protease Inhibitor. Cell *181*, 271-280 e278.

Horby, P.W., Mafham, M., Bell, J.L., Linsell, L., Staplin, N., Emberson, J., Palfreeman, A., Raw, J., Elmahi, E., Prudon, B.*, et al.* (2020). Lopinavir–ritonavir in patients admitted to hospital with COVID-19 (RECOVERY): a randomised, controlled, open-label, platform trial. The Lancet *396*, 1345-1352.

Hyseni, I., Molesti, E., Benincasa, L., Piu, P., Casa, E., Temperton, N.J., Manenti, A., and Montomoli, E. (2020). Characterisation of SARS-CoV-2 Lentiviral Pseudotypes and Correlation between Pseudotype-Based Neutralisation Assays and Live Virus-Based Micro Neutralisation Assays. Viruses *12*.

Jin, Z., Du, X., Xu, Y., Deng, Y., Liu, M., Zhao, Y., Zhang, B., Li, X., Zhang, L., Peng, C.*, et al.* (2020a). Structure of M(pro) from SARS-CoV-2 and discovery of its inhibitors. Nature *582*, 289-293.

Jin, Z., Zhao, Y., Sun, Y., Zhang, B., Wang, H., Wu, Y., Zhu, Y., Zhu, C., Hu, T., Du, X.*, et al.* (2020b). Structural basis for the inhibition of SARS-CoV-2 main protease by antineoplastic drug carmofur. Nat Struct Mol Biol *27*, 529-532.

Jordan, A., Bisgrove, D., and Verdin, E. (2003). HIV reproducibly establishes a latent infection after acute infection of T cells in vitro. EMBO J *22*, 1868-1877.

bioRxiv preprint doi: https://doi.org/10.1101/2021.03.22.435957; this version posted March 22, 2021. The copyright holder for this preprint (which was not certified by peer review) is the author/funder, who has granted bioRxiv a license to display the preprint in perpetuity. It is made available under aCC-BY 4.0 International license.

Katoh, K., Misawa, K., Kuma, K.i., and Miyata, T. (2002). MAFFT: a novel method for rapid multiple sequence alignment based on fast Fourier transform. Nucleic Acids Research *30*, 3059-3066.

Kilianski, A., Mielech, A.M., Deng, X., and Baker, S.C. (2013). Assessing activity and inhibition of Middle East respiratory syndrome coronavirus papain-like and 3C-like proteases using luciferase-based biosensors. J Virol *87*, 11955-11962.

Kim, D.K., Knapp, J.J., Kuang, D., Chawla, A., Cassonnet, P., Lee, H., Sheykhkarimli, D., Samavarchi-Tehrani, P., Abdouni, H., Rayhan, A.*, et al.* (2020). A Comprehensive, Flexible Collection of SARS-CoV-2 Coding Regions. G3 (Bethesda).

Kim, Y., Lovell, S., Tiew, K.C., Mandadapu, S.R., Alliston, K.R., Battaile, K.P., Groutas, W.C., and Chang, K.O. (2012). Broad-spectrum antivirals against 3C or 3C-like proteases of picornaviruses, noroviruses, and coronaviruses. J Virol *86*, 11754-11762.

Kneller, D.W., Phillips, G., O'Neill, H.M., Jedrzejczak, R., Stols, L., Langan, P., Joachimiak, A., Coates, L., and Kovalevsky, A. (2020). Structural plasticity of SARS-CoV-2 3CL M(pro) active site cavity revealed by room temperature X-ray crystallography. Nat Commun *11*, 3202.

Li, X., Lidsky, P., Xiao, Y., Wu, C.T., Garcia-Knight, M., Yang, J., Nakayama, T., Nayak, J.V., Jackson, P.K., Andino, R.*, et al.* (2020). Ethacridine inhibits SARS-CoV-2 by inactivating viral particles in cellular models. bioRxiv.

Lindsten, K., Uhlikova, T., Konvalinka, J., Masucci, M.G., and Dantuma, N.P. (2001). Cell-based fluorescence assay for human immunodeficiency virus type 1 protease activity. Antimicrob Agents Chemother *45*, 2616-2622.

Ma, C., Sacco, M.D., Hurst, B., Townsend, J.A., Hu, Y., Szeto, T., Zhang, X., Tarbet, B., Marty, M.T., Chen, Y.*, et al.* (2020). Boceprevir, GC-376, and calpain inhibitors II, XII inhibit SARS-CoV-2 viral replication by targeting the viral main protease. Cell Res *30*, 678-692.

Matheson, N.J., and Lehner, P.J. (2020). How does SARS-CoV-2 cause COVID-19? Science *369*, 510-511.

bioRxiv preprint doi: https://doi.org/10.1101/2021.03.22.435957; this version posted March 22, 2021. The copyright holder for this preprint (which was not certified by peer review) is the author/funder, who has granted bioRxiv a license to display the preprint in perpetuity. It is made available under aCC-BY 4.0 International license.

Menzies, S.A., Volkmar, N., van den Boomen, D.J., Timms, R.T., Dickson, A.S., Nathan, J.A., and Lehner, P.J. (2018). The sterol-responsive RNF145 E3 ubiquitin ligase mediates the degradation of HMG-CoA reductase together with gp78 and Hrd1. Elife *7*.

Miles, A.L., Burr, S.P., Grice, G.L., and Nathan, J.A. (2017). The vacuolar-ATPase complex and assembly factors, TMEM199 and CCDC115, control HIF1alpha prolyl hydroxylation by regulating cellular iron levels. Elife *6*.

Mishra, T., Sreepadmanabh, M., Ramdas, P., Sahu, A.K., Kumar, A., and Chande, A. (2021). SARS CoV-2 nucleoprotein enhances the infectivity of lentiviral spike particles. bioRxiv, 2021.2002.2011.430757.

Mlcochova, P., Collier, D., Ritchie, A., Assennato, S.M., Hosmillo, M., Goel, N., Meng, B., Chatterjee, K., Mendoza, V., Temperton, N.*, et al.* (2020). Combined Point-of-Care Nucleic Acid and Antibody Testing for SARS-CoV-2 following Emergence of D614G Spike Variant. Cell Rep Med *1*, 100099.

Nie, J., Li, Q., Wu, J., Zhao, C., Hao, H., Liu, H., Zhang, L., Nie, L., Qin, H., Wang, M.*, et al.* (2020). Quantification of SARS-CoV-2 neutralizing antibody by a pseudotyped virus-based assay. Nat Protoc *15*, 3699-3715.

O'Brien, A., Chen, D.Y., Hackbart, M., Close, B.J., O'Brien, T.E., Saeed, M., and Baker, S.C. (2021). Detecting SARS-CoV-2 3CLpro expression and activity using a polyclonal antiserum and a luciferase-based biosensor. Virology *556*, 73-78.

Papa, G., Mallery, D.L., Albecka, A., Welch, L., Cattin-Ortolá, J., Luptak, J., Paul, D., McMahon, H.T., Goodfellow, I.G., Carter, A.*, et al.* (2020). Furin cleavage of SARS-CoV-2 Spike promotes but is not essential for infection and cell-cell fusion. bioRxiv, 2020.2008.2013.243303.

Patterson, E.I., Prince, T., Anderson, E.R., Casas-Sanchez, A., Smith, S.L., Cansado-Utrilla, C., Solomon, T., Griffiths, M.J., Acosta-Serrano, A., Turtle, L.*, et al.* (2020). Methods of Inactivation of SARS-CoV-2 for Downstream Biological Assays. J Infect Dis *222*, 1462-1467.

Pedersen, N.C., Kim, Y., Liu, H., Galasiti Kankanamalage, A.C., Eckstrand, C., Groutas, W.C., Bannasch, M., Meadows, J.M., and Chang, K.O. (2018). Efficacy of a 3C-like protease inhibitor

bioRxiv preprint doi: https://doi.org/10.1101/2021.03.22.435957; this version posted March 22, 2021. The copyright holder for this preprint (which was not certified by peer review) is the author/funder, who has granted bioRxiv a license to display the preprint in perpetuity. It is made available under aCC-BY 4.0 International license.

in treating various forms of acquired feline infectious peritonitis. J Feline Med Surg *20*, 378-392.

Phillips, N. (2021). The coronavirus is here to stay - here's what that means. Nature *590*, 382-384.

Rathnayake, A.D., Zheng, J., Kim, Y., Perera, K.D., Mackin, S., Meyerholz, D.K., Kashipathy, M.M., Battaile, K.P., Lovell, S., Perlman, S.*, et al.* (2020). 3C-like protease inhibitors block coronavirus replication in vitro and improve survival in MERS-CoV-infected mice. Sci Transl Med *12*.

Rawson, J.M.O., Duchon, A., Nikolaitchik, O.A., Pathak, V.K., and Hu, W.S. (2021). Development of a Cell-Based Luciferase Complementation Assay for Identification of SARS-CoV-2 3CL(pro) Inhibitors. Viruses *13*.

Rice, P., Longden, I., and Bleasby, A. (2000). EMBOSS: the European Molecular Biology Open Software Suite. Trends Genet *16*, 276-277.

Sabariegos, R., Picazo, F., Domingo, B., Franco, S., Martinez, M.A., and Llopis, J. (2009). Fluorescence resonance energy transfer-based assay for characterization of hepatitis C virus NS3-4A protease activity in live cells. Antimicrob Agents Chemother *53*, 728-734.

Sarzotti-Kelsoe, M., Bailer, R.T., Turk, E., Lin, C.L., Bilska, M., Greene, K.M., Gao, H., Todd, C.A., Ozaki, D.A., Seaman, M.S.*, et al.* (2014). Optimization and validation of the TZM-bl assay for standardized assessments of neutralizing antibodies against HIV-1. J Immunol Methods *409*, 131-146.

Schneider, T.D., and Stephens, R.M. (1990). Sequence logos: a new way to display consensus sequences. Nucleic Acids Res *18*, 6097-6100.

Shin, D., Mukherjee, R., Grewe, D., Bojkova, D., Baek, K., Bhattacharya, A., Schulz, L., Widera, M., Mehdipour, A.R., Tascher, G.*, et al.* (2020). Papain-like protease regulates SARS-CoV-2 viral spread and innate immunity. Nature.

Simonis, A., Theobald, S.J., Fatkenheuer, G., Rybniker, J., and Malin, J.J. (2021). A comparative analysis of remdesivir and other repurposed antivirals against SARS-CoV-2. EMBO Mol Med *13*, e13105.

bioRxiv preprint doi: https://doi.org/10.1101/2021.03.22.435957; this version posted March 22, 2021. The copyright holder for this preprint (which was not certified by peer review) is the author/funder, who has granted bioRxiv a license to display the preprint in perpetuity. It is made available under aCC-BY 4.0 International license.

Stewart, S.A., Dykxhoorn, D.M., Palliser, D., Mizuno, H., Yu, E.Y., An, D.S., Sabatini, D.M., Chen, I.S., Hahn, W.C., Sharp, P.A., *et al.* (2003). Lentivirus-delivered stable gene silencing by RNAi in primary cells. RNA *9*, 493-501.

Tchasovnikarova, I.A., Timms, R.T., Matheson, N.J., Wals, K., Antrobus, R., Gottgens, B., Dougan, G., Dawson, M.A., and Lehner, P.J. (2015). GENE SILENCING. Epigenetic silencing by the HUSH complex mediates position-effect variegation in human cells. Science *348*, 1481-1485.

To, T.L., Piggott, B.J., Makhijani, K., Yu, D., Jan, Y.N., and Shu, X. (2015). Rationally designed fluorogenic protease reporter visualizes spatiotemporal dynamics of apoptosis in vivo. Proc Natl Acad Sci U S A *112*, 3338-3343.

V'Kovski, P., Kratzel, A., Steiner, S., Stalder, H., and Thiel, V. (2020). Coronavirus biology and replication: implications for SARS-CoV-2. Nat Rev Microbiol.

van den Boomen, D.J.H., Sienkiewicz, A., Berlin, I., Jongsma, M.L.M., van Elsland, D.M., Luzio, J.P., Neefjes, J.J.C., and Lehner, P.J. (2020). A trimeric Rab7 GEF controls NPC1-dependent lysosomal cholesterol export. Nat Commun *11*, 5559.

Vuong, W., Khan, M.B., Fischer, C., Arutyunova, E., Lamer, T., Shields, J., Saffran, H.A., McKay, R.T., van Belkum, M.J., Joyce, M.A., *et al.* (2020). Feline coronavirus drug inhibits the main protease of SARS-CoV-2 and blocks virus replication. Nat Commun *11*, 4282.

Walensky, R.P., Walke, H.T., and Fauci, A.S. (2021). SARS-CoV-2 Variants of Concern in the United States-Challenges and Opportunities. JAMA.

Wang, M., Cao, R., Zhang, L., Yang, X., Liu, J., Xu, M., Shi, Z., Hu, Z., Zhong, W., and Xiao, G. (2020). Remdesivir and chloroquine effectively inhibit the recently emerged novel coronavirus (2019-nCoV) in vitro. Cell Res *30*, 269-271.

Wei, X., Decker, J.M., Liu, H., Zhang, Z., Arani, R.B., Kilby, J.M., Saag, M.S., Wu, X., Shaw, G.M., and Kappes, J.C. (2002). Emergence of resistant human immunodeficiency virus type 1 in patients receiving fusion inhibitor (T-20) monotherapy. Antimicrob Agents Chemother *46*, 1896-1905.

bioRxiv preprint doi: https://doi.org/10.1101/2021.03.22.435957; this version posted March 22, 2021. The copyright holder for this preprint (which was not certified by peer review) is the author/funder, who has granted bioRxiv a license to display the preprint in perpetuity. It is made available under aCC-BY 4.0 International license.

WHO, S.T.C. (2020). Repurposed Antiviral Drugs for Covid-19 — Interim WHO Solidarity Trial Results. New England Journal of Medicine *384*, 497-511.

Wigdal, S.S., Anderson, J.L., Vidugiris, G.J., Shultz, J., Wood, K.V., and Fan, F. (2008). A novel bioluminescent protease assay using engineered firefly luciferase. Curr Chem Genomics *2*, 16-28.

Williams, T.C., and Burgers, W.A. (2021). SARS-CoV-2 evolution and vaccines: cause for concern? Lancet Respir Med.

Xie, X., Muruato, A., Lokugamage, K.G., Narayanan, K., Zhang, X., Zou, J., Liu, J., Schindewolf, C., Bopp, N.E., Aguilar, P.V.*, et al.* (2020a). An Infectious cDNA Clone of SARS-CoV-2. Cell Host Microbe *27*, 841-848 e843.

Xie, X., Muruato, A.E., Zhang, X., Lokugamage, K.G., Fontes-Garfias, C.R., Zou, J., Liu, J., Ren, P., Balakrishnan, M., Cihlar, T.*, et al.* (2020b). A nanoluciferase SARS-CoV-2 for rapid neutralization testing and screening of anti-infective drugs for COVID-19. Nat Commun *11*, 5214.

Yan, S., and Wu, G. (2021). Spatial and temporal roles of SARS-CoV PL(pro) -A snapshot. FASEB J *35*, e21197.

Zhang, Q., Schepis, A., Huang, H., Yang, J., Ma, W., Torra, J., Zhang, S.Q., Yang, L., Wu, H., Nonell, S.*, et al.* (2019). Designing a Green Fluorogenic Protease Reporter by Flipping a Beta Strand of GFP for Imaging Apoptosis in Animals. J Am Chem Soc *141*, 4526-4530.

bioRxiv preprint doi: https://doi.org/10.1101/2021.03.22.435957; this version posted March 22, 2021. The copyright holder for this preprint (which was not certified by peer review) is the author/funder, who has granted bioRxiv a license to display the preprint in perpetuity. It is made available under aCC-BY 4.0 International license.

A

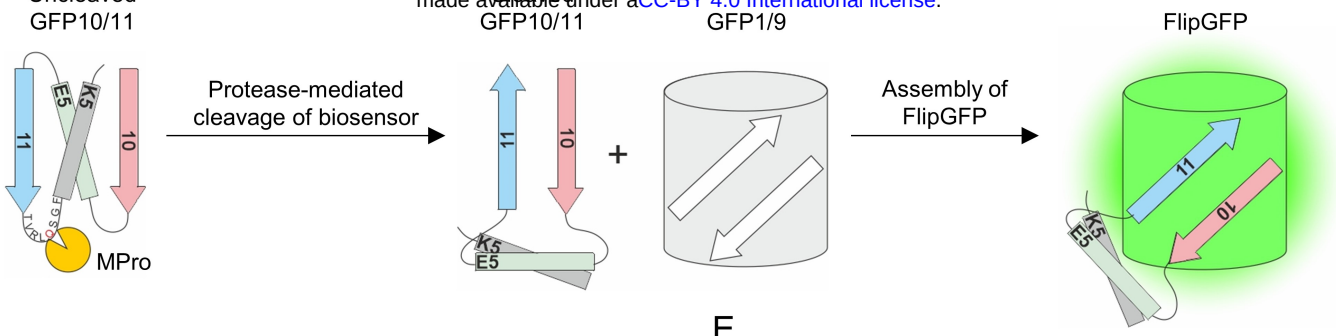

B

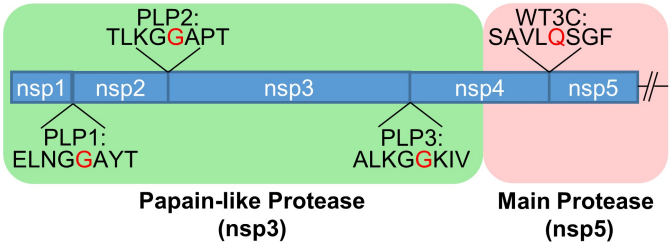

C

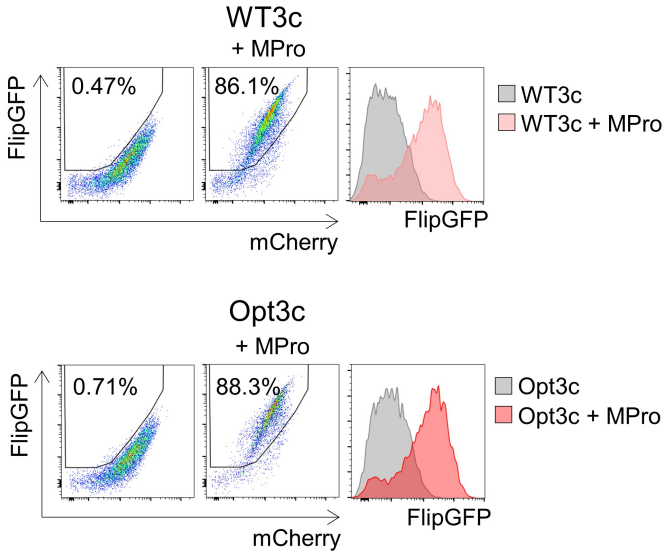

E

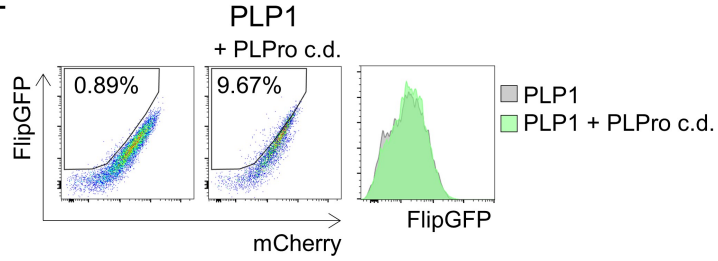

D

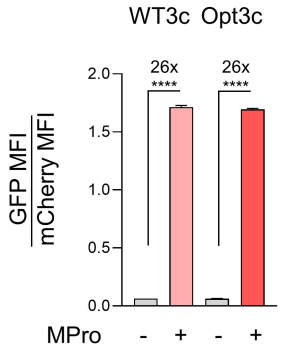

F

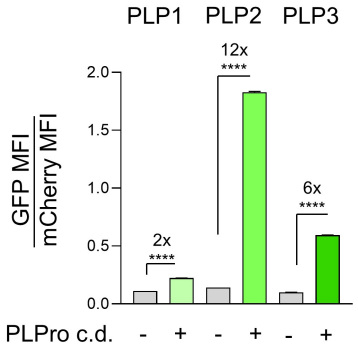

G

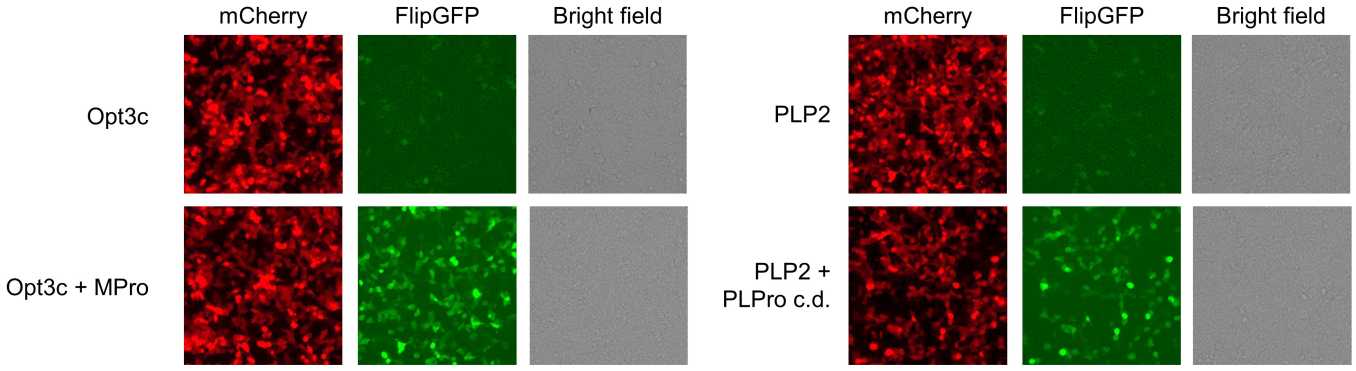

Figure 1

bioRxiv preprint doi: https://doi.org/10.1101/2021.03.22.435957; this version posted March 22, 2021. The copyright holder for this preprint (which was not certified by peer review) is the author/funder, who has granted bioRxiv a license to display the preprint in perpetuity. It is made available under aCC-BY 4.0 International license.

A

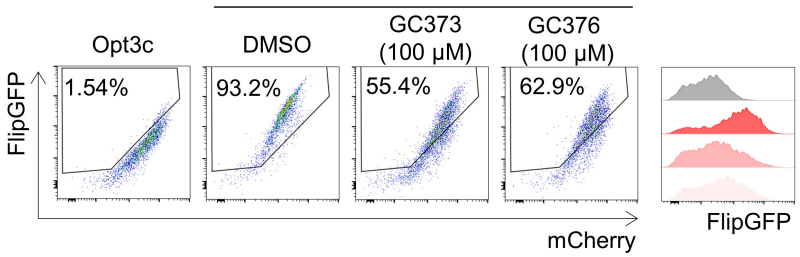

B

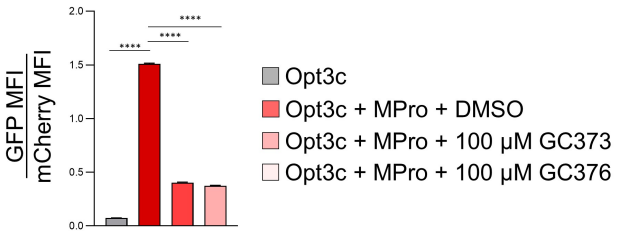

C

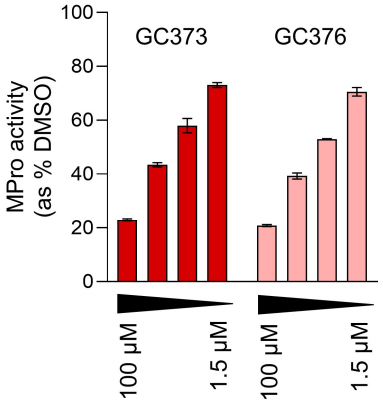

D

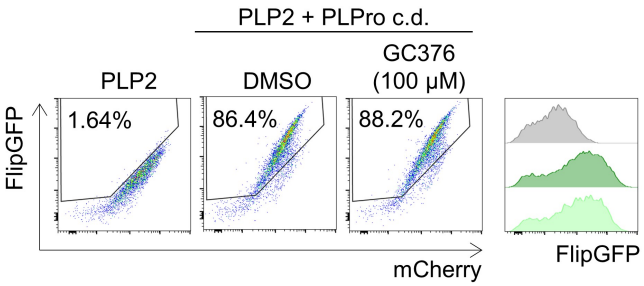

E

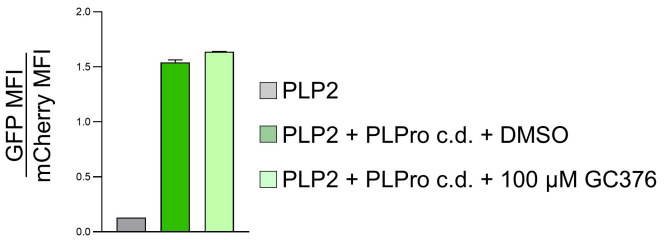

F

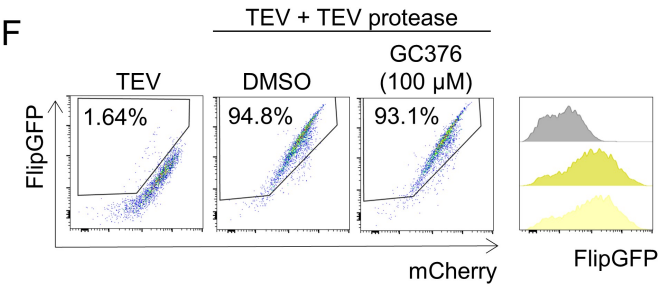

G

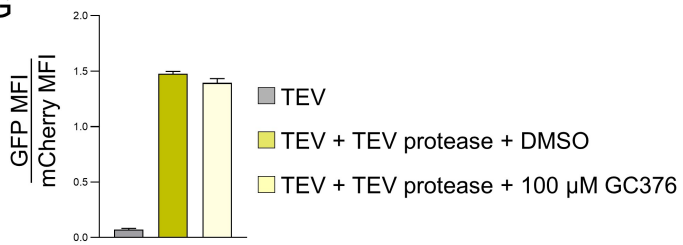

Figure 2

bioRxiv preprint doi: https://doi.org/10.1101/2021.03.22.435957; this version posted March 22, 2021. The copyright holder for this preprint (which was not certified by peer review) is the author/funder, who has granted bioRxiv a license to display the preprint in perpetuity. It is made available under aCC-BY 4.0 International license.

A

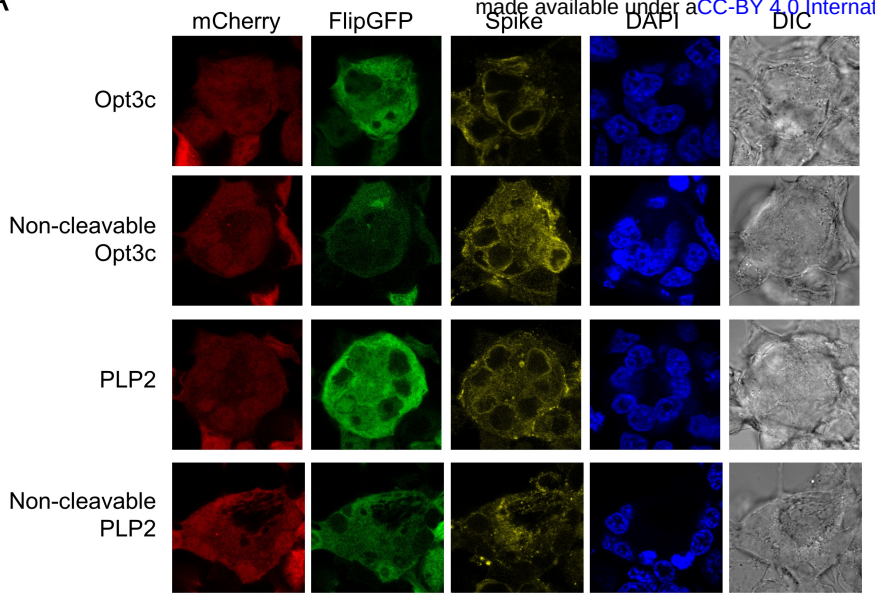

B

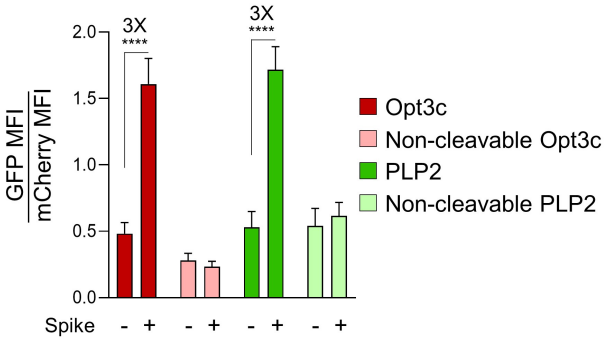

C

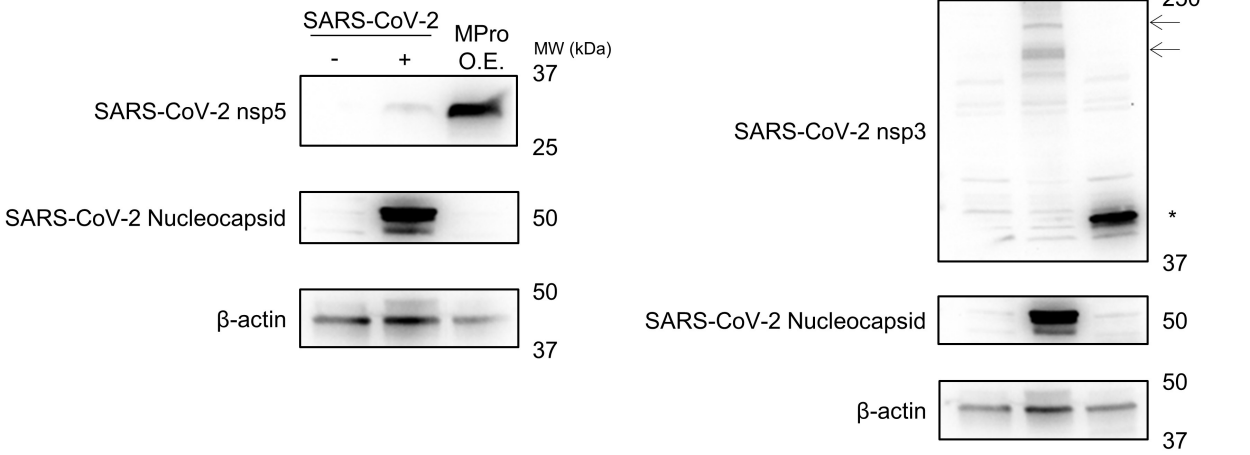

Figure 3

bioRxiv preprint doi: https://doi.org/10.1101/2021.03.22.435957; this version posted March 22, 2021. The copyright holder for this preprint (which was not certified by peer review) is the author/funder, who has granted bioRxiv a license to display the preprint in perpetuity. It is made available under aCC-BY 4.0 International license.

A

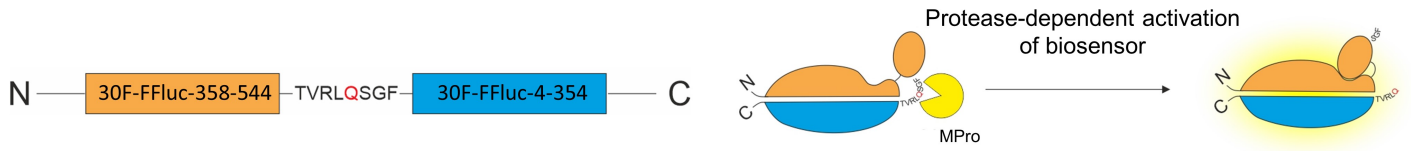

B

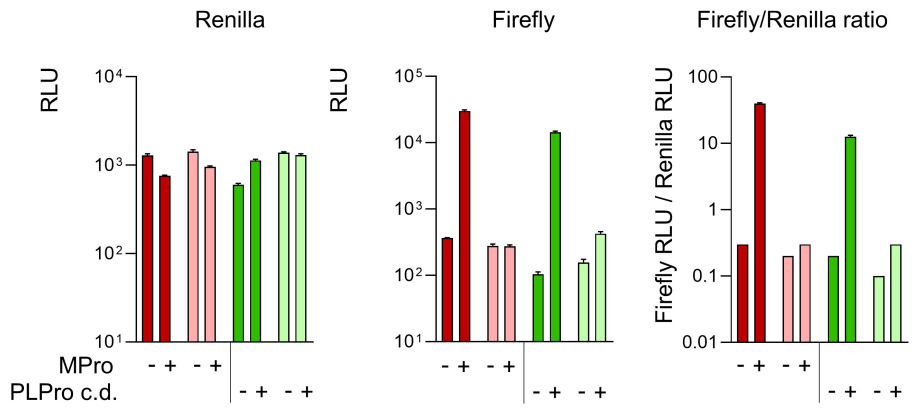

C

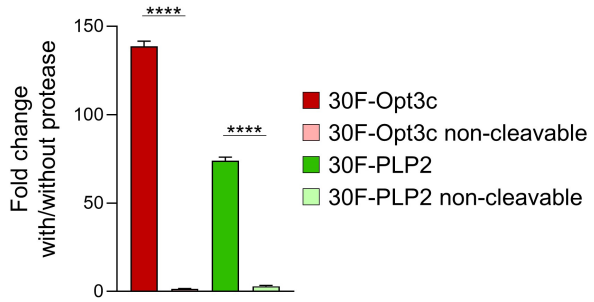

D

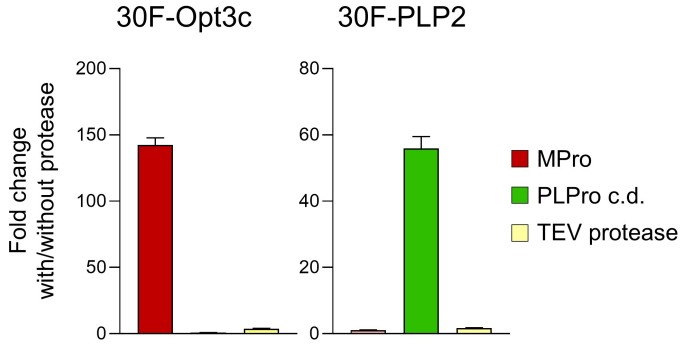

Figure 4

bioRxiv preprint doi: https://doi.org/10.1101/2021.03.22.435957; this version posted March 22, 2021. The copyright holder for this preprint (which was not certified by peer review) is the author/funder, who has granted bioRxiv a license to display the preprint in perpetuity. It is made available under a CC-BY 4.0 International license.

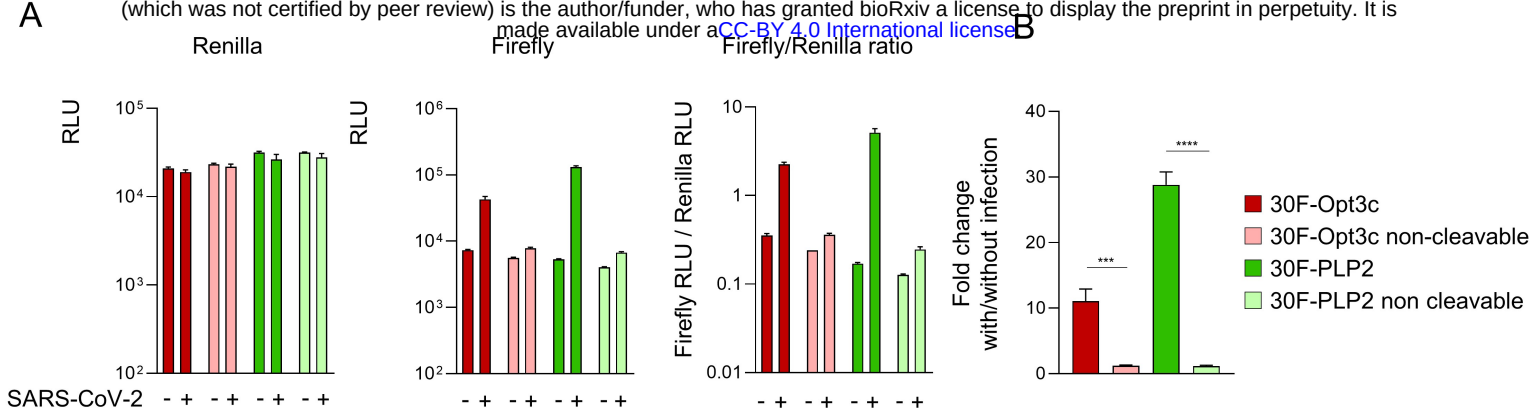

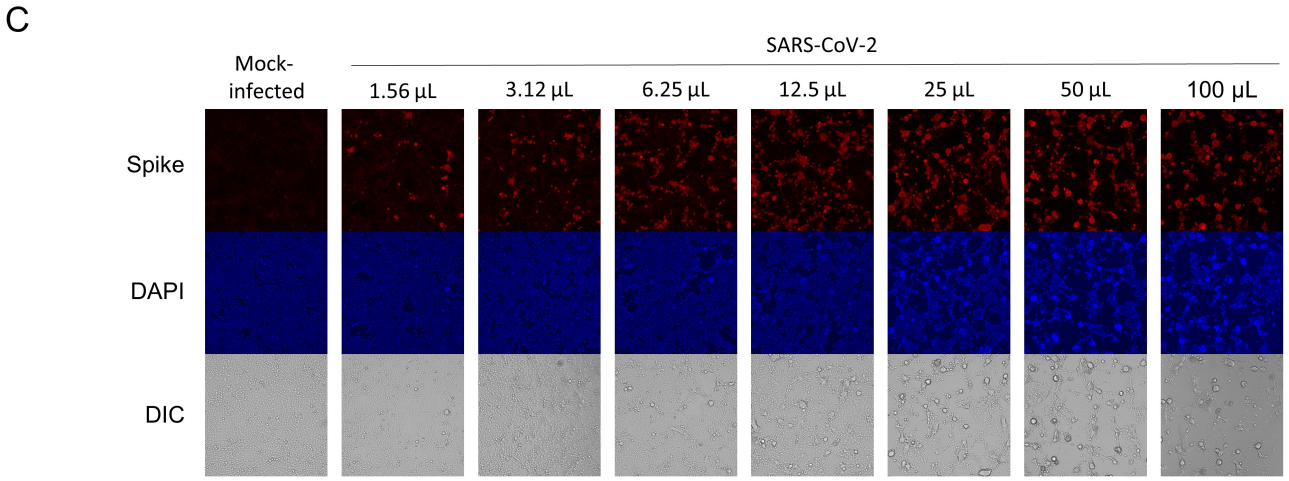

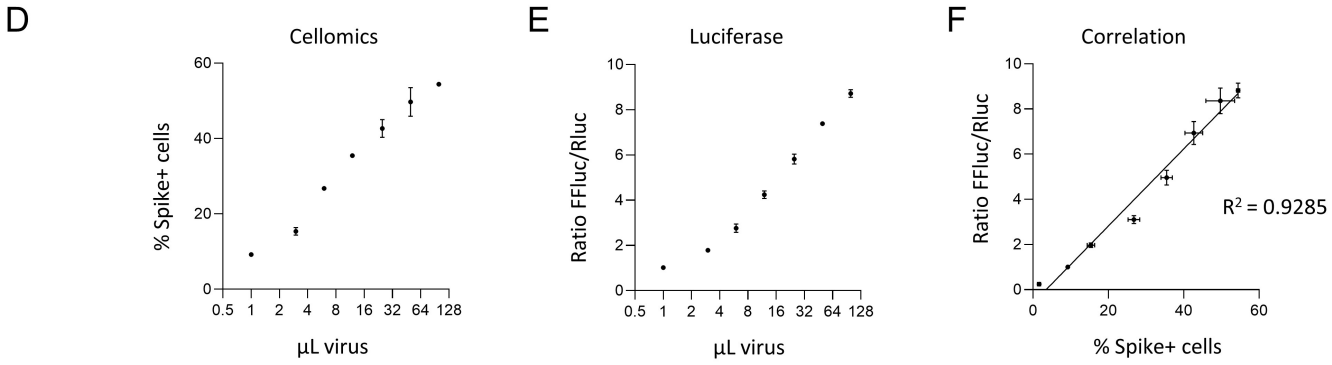

Figure 5

bioRxiv preprint doi: https://doi.org/10.1101/2021.03.22.435957; this version posted March 22, 2021. The copyright holder for this preprint (which was not certified by peer review) is the author/funder, who has granted bioRxiv a license to display the preprint in perpetuity. It is made available under aCC-BY 4.0 International license.

A

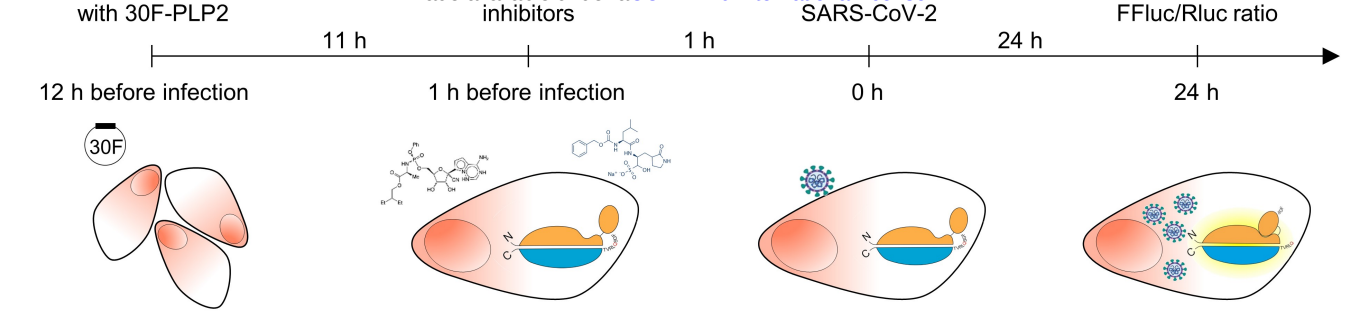

B

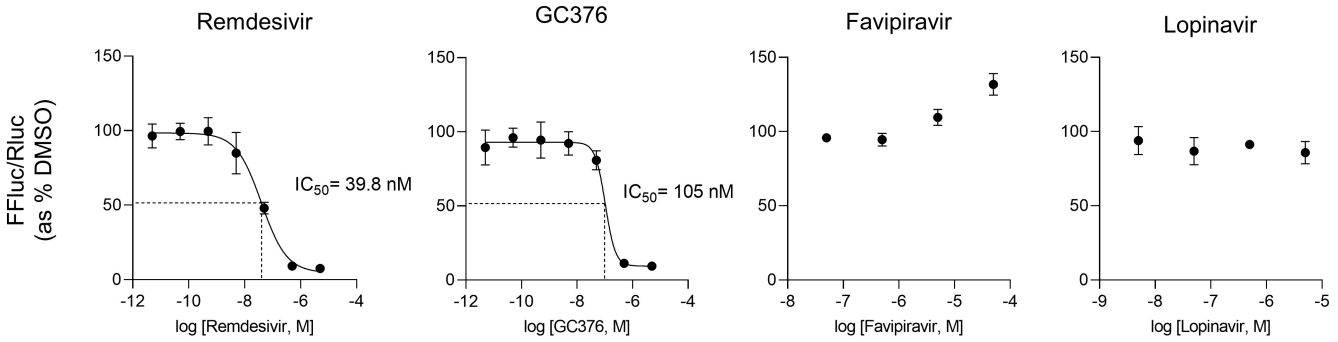

Figure 6

bioRxiv preprint doi: https://doi.org/10.1101/2021.03.22.435957; this version posted March 22, 2021. The copyright holder for this preprint (which was not certified by peer review) is the author/funder, who has granted bioRxiv a license to display the preprint in perpetuity. It is made available under aCC-BY 4.0 International license.

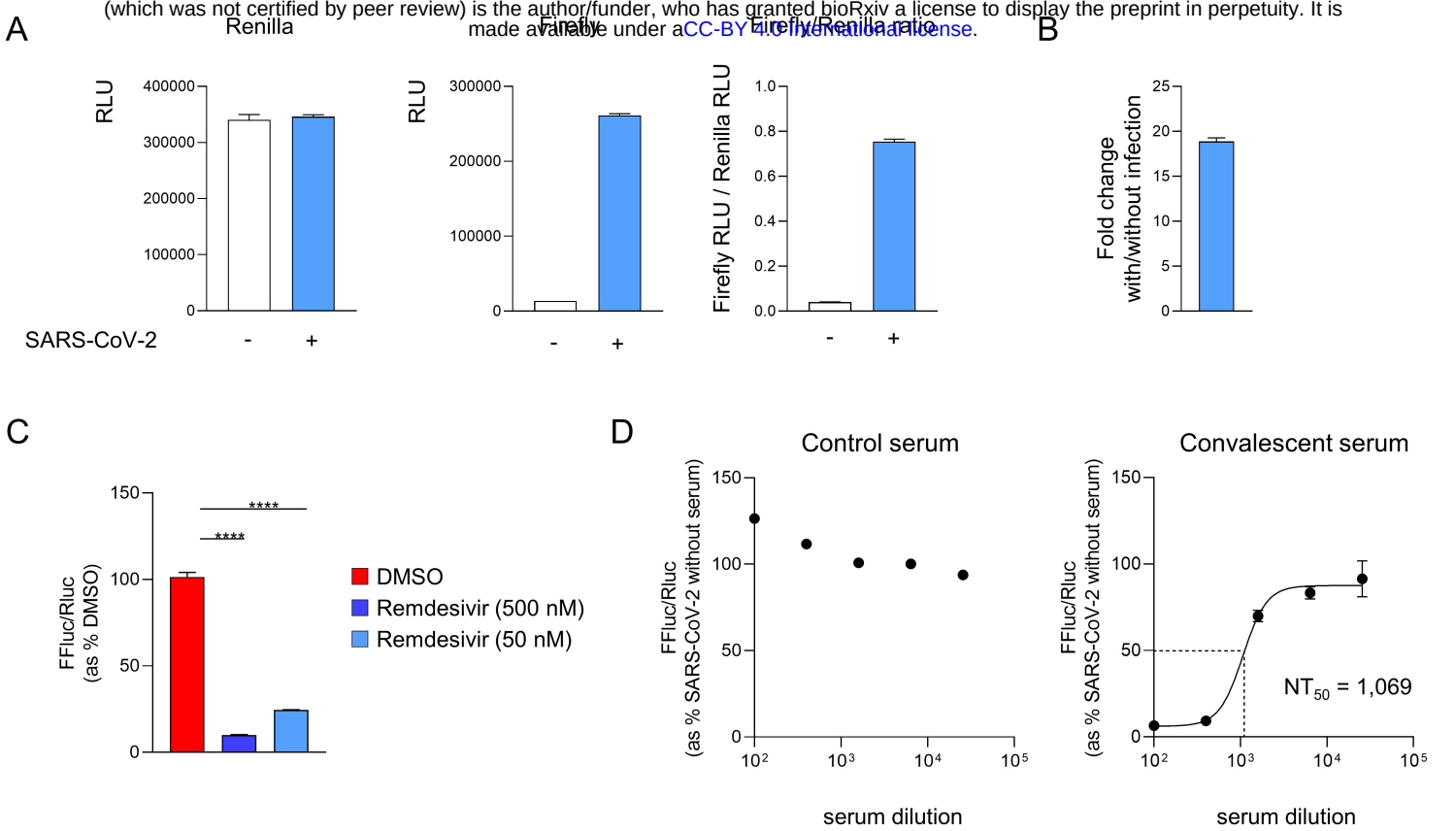

Figure 7

bioRxiv preprint doi: https://doi.org/10.1101/2021.03.22.435957; this version posted March 22, 2021. The copyright holder for this preprint (which was not certified by peer review) is the author/funder, who has granted bioRxiv a license to display the preprint in perpetuity. It is made available under a CC-BY 4.0 International license.

A

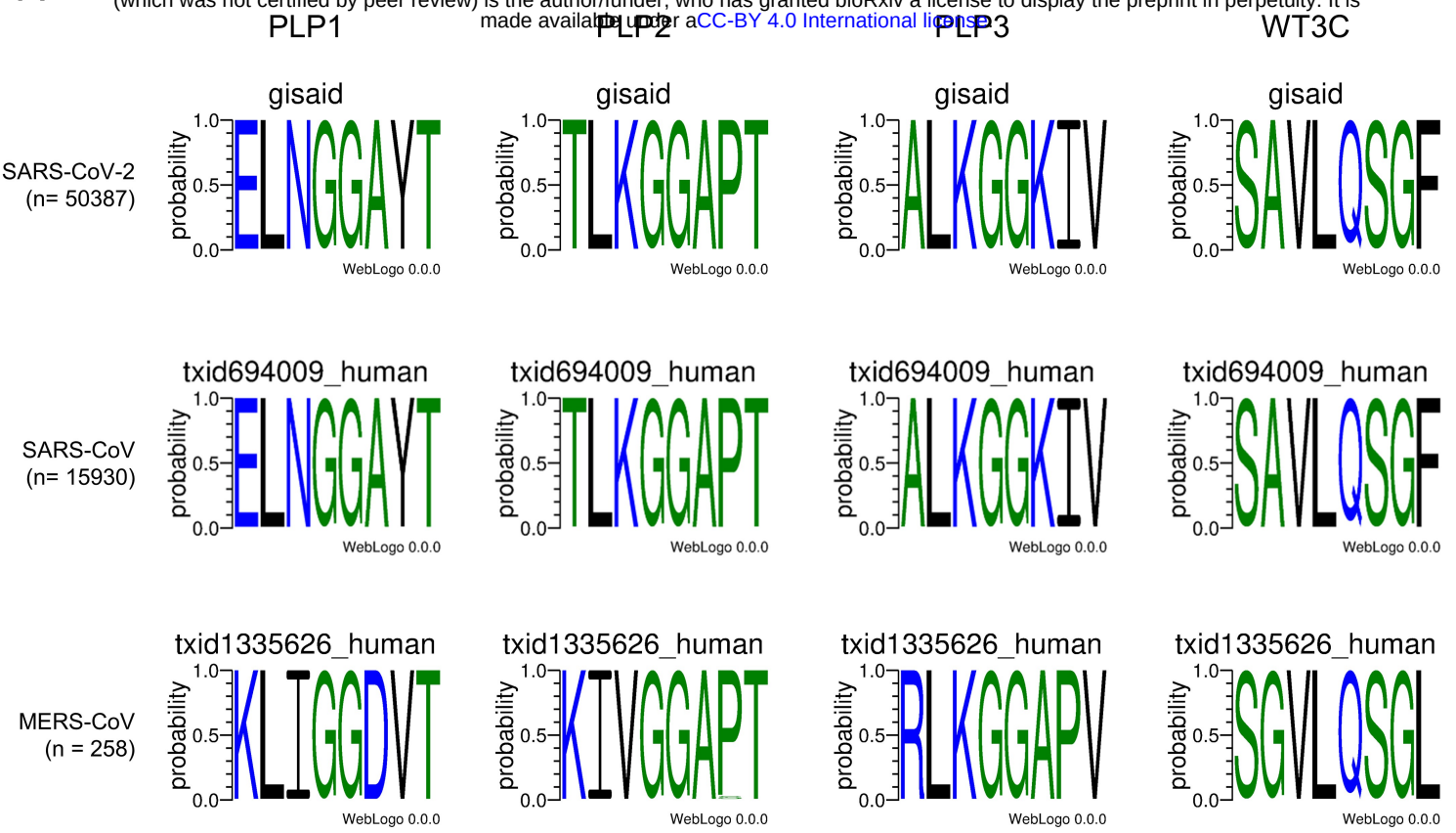

B

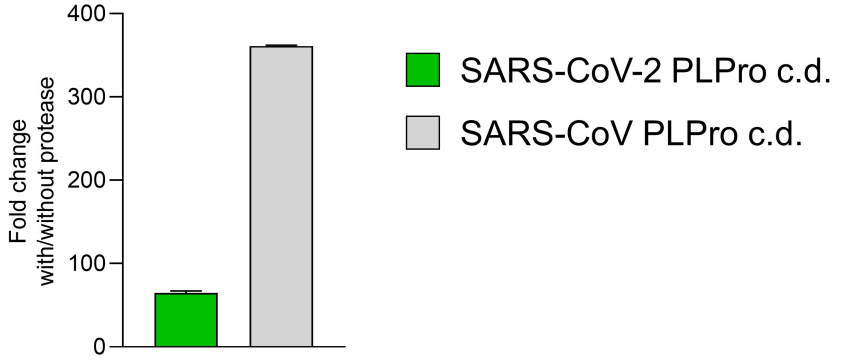

Figure 1 – figure supplement 1

bioRxiv preprint doi: https://doi.org/10.1101/2021.03.22.435957; this version posted March 22, 2021. The copyright holder for this preprint (which was not certified by peer review) is the author/funder, who has granted bioRxiv a license to display the preprint in perpetuity. It is made available under aCC-BY 4.0 International license.

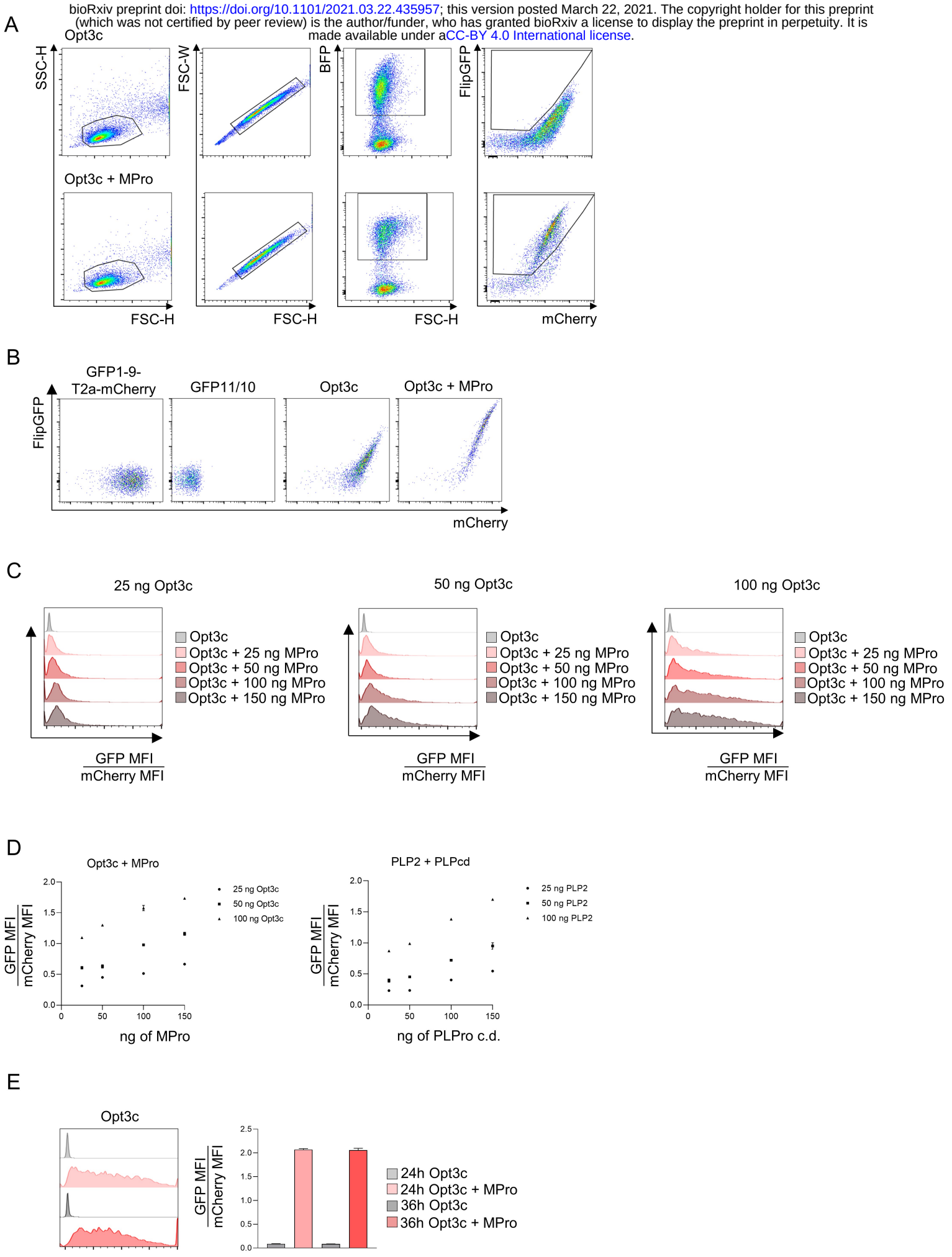

Figure 1 – figure supplement 2

bioRxiv preprint doi: https://doi.org/10.1101/2021.03.22.435957; this version posted March 22, 2021. The copyright holder for this preprint (which was not certified by peer review) is the author/funder, who has granted bioRxiv a license to display the preprint in perpetuity. It is made available under aCC-BY 4.0 International license.

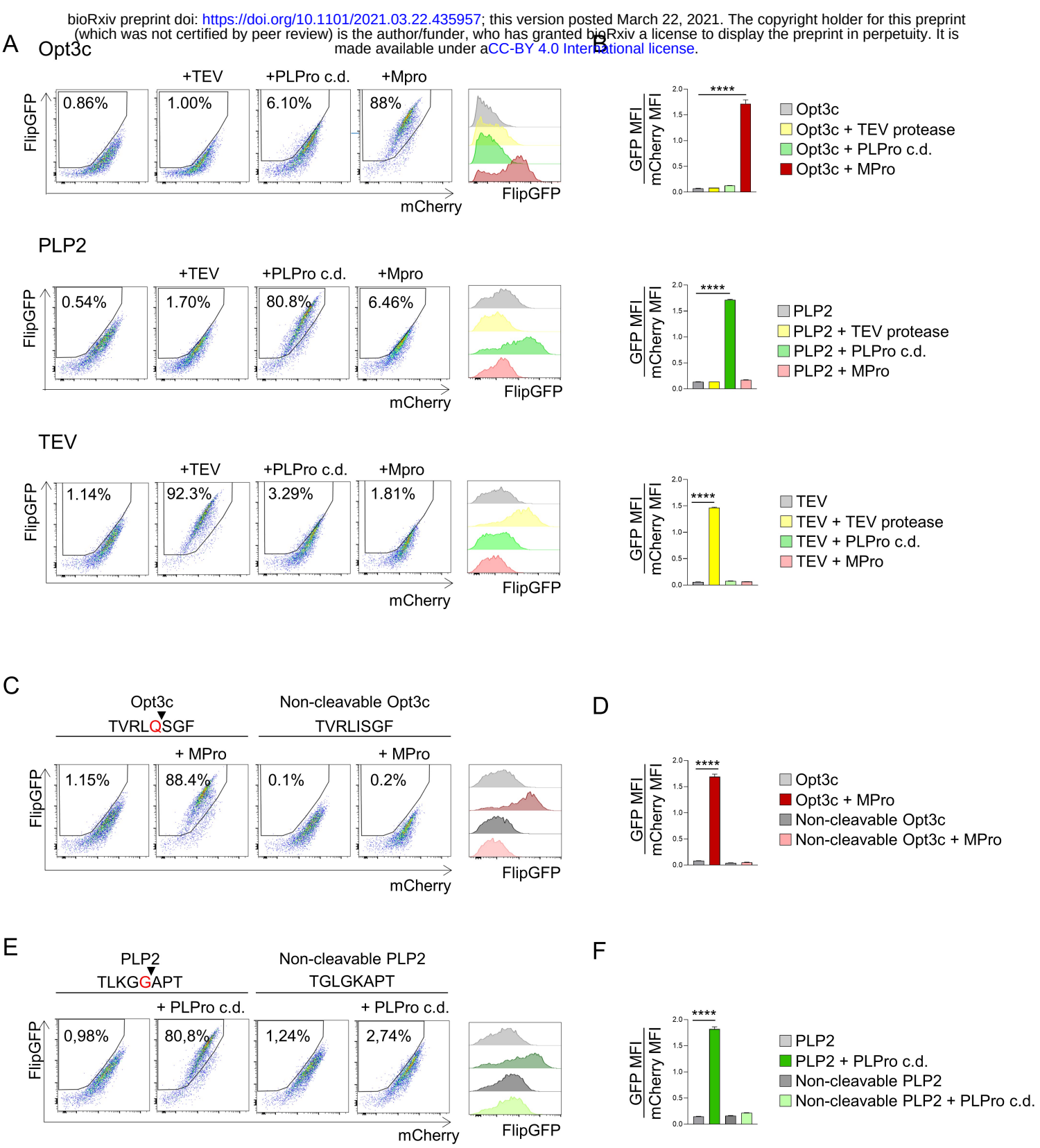

Figure 1 – figure supplement 3

bioRxiv preprint doi: https://doi.org/10.1101/2021.03.22.435957; this version posted March 22, 2021. The copyright holder for this preprint (which was not certified by peer review) is the author/funder, who has granted bioRxiv a license to display the preprint in perpetuity. It is made available under aCC-BY 4.0 International license.

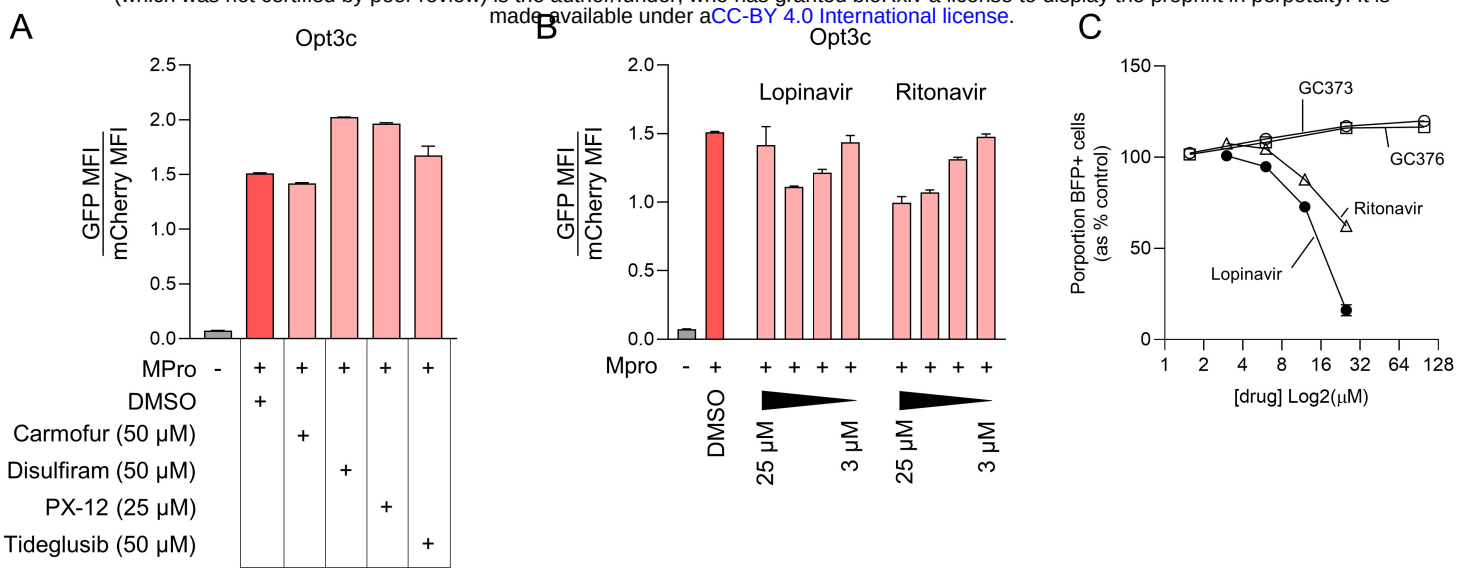

Figure 2 – figure supplement 1

bioRxiv preprint doi: https://doi.org/10.1101/2021.03.22.435957; this version posted March 22, 2021. The copyright holder for this preprint (which was not certified by peer review) is the author/funder, who has granted bioRxiv a license to display the preprint in perpetuity. It is made available under aCC-BY 4.0 International license.

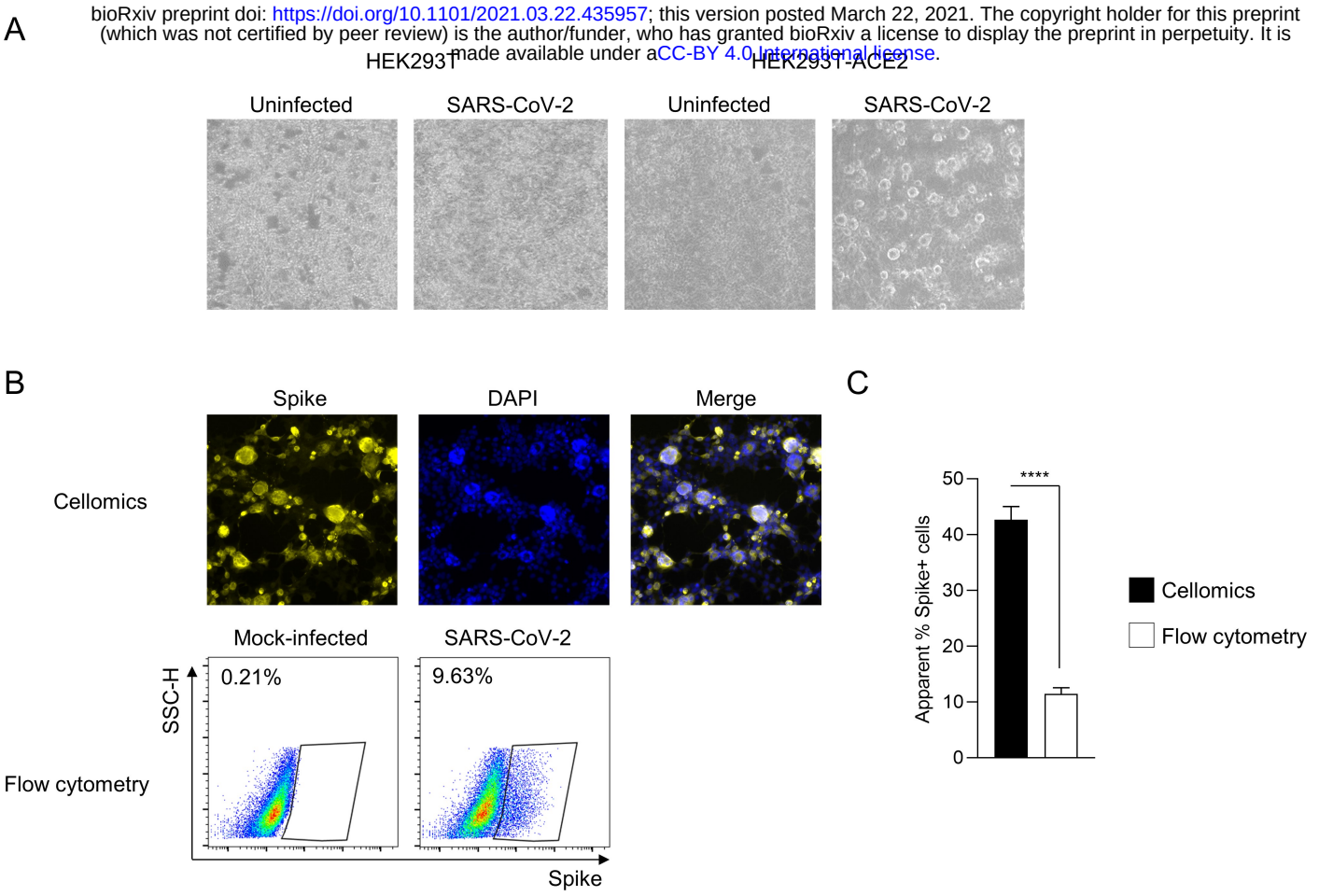

Figure 3 – figure supplement 1

bioRxiv preprint doi: https://doi.org/10.1101/2021.03.22.435957; this version posted March 22, 2021. The copyright holder for this preprint (which was not certified by peer review) is the author/funder, who has granted bioRxiv a license to display the preprint in perpetuity. It is made available under aCC-BY 4.0 International license.

A

pGIo-30F-PLP2

pHRSIN-30F-PLP2-IRES-hRluc-WPRE-PGK-Puro

Figure 7 – figure supplement 1